The Astrophysical Journal, 607:982–998, 2004 June 1

THIRTY-FIVE NEW PULSATING DA WHITE DWARF STARS

Anjum S. Mukadam,[1,2] F. Mullally,[1,2] R. E. Nather,[1,2] D. E. Winget,[1,2] Ted von Hippel,[1,2] S. J. Kleinman,[3] Atsuko Nitta,[3] Jurek Krzesiński,[3,4] S. O. Kepler,[5] A. Kanaan,[6] D. Koester,[7] D. J. Sullivan,[8] D. Homeier,[9] S. E. Thompson,[10] D. Reaves,[1] C. Cotter,[1] D. Slaughter,[1] and J. Brinkmann[3]

Received 2003 November 7; accepted 2004 January 21

ABSTRACT

We present 35 new pulsating DA (hydrogen atmosphere) white dwarf stars discovered from the Sloan Digital Sky Survey (SDSS) and the Hamburg Quasar Survey (HQS). We have acquired high-speed time series photometry of preselected DA white dwarfs with a prime focus CCD photometer on the 2.1 m telescope at McDonald Observatory over 15 months. We selected these stars on the basis of prior photometric and spectroscopic observations by the SDSS and HQS. For the homogeneous SDSS sample, we achieve a success rate of 80% for finding new variables at a detection threshold of 0.1%–0.3%. With 35 newly discovered DA variable white dwarfs, we almost double the current sample of 39.

Subject headings: stars: imaging — stars: oscillations — stars: variables: other — techniques: photometric — white dwarfs

1. INTRODUCTION

White dwarfs are the evolutionary end points of most stars in the universe, and their structures provide constraints on their prior evolution. Their high gravities and temperatures make them good cosmic laboratories for the study of physics under extreme conditions. Pulsations are seen along the white dwarf cooling track in three temperature regions and are believed to be an evolutionary effect in otherwise normal white dwarfs (Robinson 1979; Fontaine et al. 1985, 2003). As the white dwarfs pass through these instability strips, we observe them as nonradial g-mode pulsators (see the review paper Winget 1998 and references therein). Asteroseismology is the technique of using these global pulsations to probe the stellar interiors.

Since 80% of all white dwarf stars have atmospheres dominated by hydrogen (DAs; Fleming et al. 1986), to understand the DA variables (DAVs) is to understand the most common type of white dwarf. The DAVs, also known as ZZ Ceti stars, are observed to pulsate in the temperature range of 11,000–12,500 K for $\log g \approx 8$ (Bergeron et al. 1995; Koester & Allard 2000). The pulsation periods range from $\sim$100 to 1200 s and are consistent with nonradial g-mode pulsations. Pulsation modes in a spherical gravitational potential can be characterized by a unique set of indices (k, l, m), similar to the quantum numbers that describe the state of a bound electron in the spherical electrostatic potential of a nucleus. The mode indices l and m are associated with spherical harmonics, and k corresponds to the radial quantum number (see Winget 1998).

The pulsation periods and amplitudes of the DAV stars show a distinct trend with temperature (Clemens 1993 and references therein). The hot DAVs (hDAVs) in the hotter half of the instability strip show relatively few pulsation modes, with low amplitudes ($\sim$0.1%–3%) and periods around 100–300 s. The cooler DAVs (cDAVs) show longer periods, around 600–1000 s, larger amplitudes (up to 30%), and greater amplitude variability (Kleinman et al. 1998). This well-established period-temperature and amplitude-temperature correlation allows us to classify DAV stars meaningfully into the hDAVs and the cDAVs (see § 6 for further discussion).

2. MOTIVATION: WHY SEARCH FOR DAVs?

Understanding the structure and evolution of a statistically significant sample of DAVs has implications for other areas of astronomy, some of which are discussed below:

2.1. *Stellar Structure*

Each pulsation mode is an independent constraint on the structure of the star; the more modes we detect, the better our understanding of the stellar structure. Apart from our current search, there are 39 DAVs in the literature (see Bergeron et al. 2004; Warner & Woudt 2003); additional pulsators and additional modes will help us understand the DAVs as a class.

We can probe stellar structure and composition by finding a single star rich in pulsation modes and/or by finding a large number of pulsators to use the method of ensemble asteroseismology. We can determine stellar mass, core composition, age, rotation rate, magnetic field strength, and parallax using asteroseismology. Measuring the rotation period for DAVs and comparing it with other classes of white dwarf pulsators at different temperatures can give us clues about the evolution of angular momentum. The carbon-oxygen ratio in white dwarf cores contains the rate of the astrophysically important, but experimentally uncertain, $^{12}C(\alpha,\gamma)^{16}O$ nuclear reaction (Metcalfe 2003; Metcalfe et al. 2002).

A search for a large number of DAVs is bound to yield extreme-mass pulsators. Low-mass ($\log g \leq 7.6$) DAVs could

[1] Department of Astronomy, University of Texas at Austin, Austin, TX 78712; anjum@astro.as.utexas.edu.
[2] McDonald Observatory, Fort Davis, TX 79734.
[3] Apache Point Observatory, P.O. Box 59, Sunspot, NM 88349.
[4] Mount Suhora Observatory, Cracow Pedagogical University, ul. Podchorążych 2, 30-084 Cracow, Poland.
[5] Instituto de Física, Universidade Federal do Rio Grande do Sul, 91501-970 Porto Alegre, RS, Brazil.
[6] Departamento de Física, Universidade Federal de Santa Catarina, 88040-900, Florianopolis, SC, Brazil.
[7] Institut für Theoretische Physik und Astrophysik, Universität Kiel, 24098 Kiel, Germany.
[8] School of Chemical and Physical Sciences, Victoria University of Wellington, P.O. Box 600, Wellington, New Zealand.
[9] University of Georgia, Athens, GA 30602.
[10] Department of Physics and Astronomy, University of North Carolina, Chapel Hill, NC 27599.

well be helium core white dwarfs; pulsating He core white dwarfs should allow us to probe their equation of state. High-mass ($\log g \geq 8.5$) DAVs are potentially crystallized, paving the way for the first possible empirical test of the theory of crystallization in stellar plasma (see 2.3.2). This should also have implications for models of neutron stars and pulsars, which are thought to have crystalline crusts.

2.2. *Stable Clocks Can Be Used to Find Planets*

Hot DAVs such as G117-B15A, R548 (ZZ Ceti), and L19-2 have been monitored since 1970. The dominant mode ($l = 1$, $k = 2$) in these stars has been found to exhibit extreme amplitude and frequency stability, implying that they can serve as reliable clocks. The unidirectional drift rate of these clocks has been constrained to be smaller than a few times 10^{-15} s s^{-1} (O'Donoghue & Warner 1987; Kepler et al. 2000; Mukadam et al. 2003b). To put this number in perspective, these clocks are expected to lose one cycle in a few billion years. Clemens (1993) showed that the hDAVs form a homogeneous class, and on the basis of his work we expect that all hDAVs should show comparable frequency stability at least for this mode. Should such stable clocks have an orbiting planet around them, their reflex motion around the center of mass of the system would become measurable, providing a means of detecting the planet (e.g., Mukadam et al. 2001; Winget et al. 2003; Kepler et al. 1991). These hDAVs were once main-sequence stars, suitable hosts for planet formation. Some theoretical work indicates outer terrestrial planets and gas giants will survive the red giant phase (e.g., Vassiliadis & Wood 1993) with orbits stable on timescales longer than a fraction of a billion years (Duncan & Lissauer 1998). These timescales are comparable to the cooling time required by a newly formed white dwarf to reach the pulsational DAV strip. The success of a planet search around these stable clocks rests on finding a statistically significant number of hDAV stars.

2.3. *Seismology of DAVs Helps Reduce Uncertainties in White Dwarf Cosmochronometry*

White dwarfs at $T_{\rm eff} \sim 4500$ K are among the oldest stars in the solar neighborhood. As 98%–99% of all main-sequence stars will eventually become white dwarfs (Weidemann 1990), we can use these chronometers to determine the ages of the Galactic disk and halo (e.g., Winget et al. 1987; Hansen et al. 2002). This method, known as white dwarf cosmochronometry, has a different source of uncertainties and model assumptions than main-sequence stellar evolution. The white dwarf luminosity function also places an upper limit on the rate of change of the gravitational constant (Isern et al. 2002).

Most of the theoretical uncertainty in the age estimation of white dwarfs comes from uncalibrated model cooling rates and effects like crystallization and phase separation, which delay white dwarf cooling by releasing latent heat. The outer nondegenerate layers and the core composition play an important role in dictating the cooling rates. Although these cool white dwarfs ($T_{\rm eff} \sim 4500$ K) have not been observed to pulsate, we can still use asteroseismology to calibrate theoretical cooling curves, thus reducing the uncertainties in determining white dwarf ages.

2.3.1. *Stable Pulsators Provide a Calibration of White Dwarf Cooling Curves*

There are two competing internal evolutionary processes that govern the change in pulsation period with time ($\dot{P}$) for a single mode in the models of the ZZ Ceti stars. Cooling of the star increases the periods as a result of the increasing degeneracy, and residual gravitational contraction decreases the periods (Winget et al. 1983). Kepler et al. (2000) conclude that the rate of cooling dominates the drift rate ($\dot{P} = dP/dt$) for the DAV stars. Since at least the $l = 1$, $k = 2$ mode is expected to show extreme amplitude and frequency stability in all hDAVs, we can monitor these stars to obtain meaningful measurements of their cooling rates. Cooling rates for a large sample of hDAVs with different masses and internal compositions will prove fruitful in calibrating the DA white dwarf cooling curves. Note that a stable clock with an orbital companion will show both the parabolic cooling and the periodic variations due to the companion (see Mukadam et al. 2001); these effects are discernible and will most likely have different timescales.

2.3.2. *Massive Pulsators Help Us Study Crystallization*

For a 0.6 $M_{\odot}$ model white dwarf ($\log g \approx 8.0$), the onset of crystallization begins at $T_{\rm eff} = 6000$ K for a carbon core and at $T_{\rm eff} = 7200$ K for an oxygen core (Wood 1992). These temperatures are well below the cool edge of the DAV instability strip, implying that ordinarily we cannot study effects such as crystallization using asteroseismology. However, because of the larger central pressures in massive solar mass pulsators ($\log g \approx 8.6$), they should be substantially crystallized even at 12,000 K (Winget et al. 1997; Montgomery & Winget 1999). These variables can provide the first test of the theory of crystallization in stellar plasma. Crystallization affects the cooling rate of a white dwarf by releasing latent heat (Van Horn 1968). Theoretical calculations also suggest that some phase separation occurs between carbon and oxygen, providing an additional energy source, which delays the cooling of the star (Montgomery et al. 1999; Isern et al. 2000). Our ignorance of stellar crystallization and phase separation is the largest source of uncertainty when white dwarfs are used as chronometers to determine the age of the Galactic disk.

2.3.3. *Hydrogen Layer Masses from DAV Seismology Help Improve Models*

The outer nondegenerate layers control the rate at which the residual thermal energy of the core is radiated into space. Poorly determined hydrogen mass fractions increase the uncertainty of white dwarf ages (Wood 1990). Although we can utilize pulsating white dwarfs to measure cooling rates directly, we can do so only in select temperature ranges. Hence, determining hydrogen layer masses from asteroseismology will be helpful in improving our models and better determining white dwarf ages.

2.4. *Asteroseismological Distances from a Flickering Candle*

Obtaining a unique model fit to the pulsation modes allows us to determine an asteroseismological distance by matching the observed luminosity of the star with the model luminosity. Typically, the asteroseismological distance is more accurate than what we determine from measured parallax (e.g., Petersen & Hog 1998; Bradley 2001). Variable white dwarfs with a rich pulsation spectrum should therefore be of great interest for an independent calibration of the Galactic distance scale.

Alternatively, Salaris et al. (2001) derived distances to globular clusters by fitting a local template DA white dwarf sequence to the cluster counterpart. Uncertainties in this technique can be reduced via asteroseismology by measuring

stellar masses and hydrogen layer thicknesses for DA pulsators and extending the results systematically to other DAs.

2.5. *Establishing the ZZ Ceti Instability Strip*

Pulsation models indicate that the limits of the ZZ Ceti instability strip depend on the effective temperature and mass of the star (Bradley & Winget 1994). This was observationally confirmed by Giovannini et al. (1998) and Bergeron et al. (2004). Most model atmospheres of DAV stars treat convection with a mixing-length prescription, assuming some parameterization, the choice of which can shift the edges of the instability strip in temperature by a few $\times 1000$ K (Bergeron et al. 1995; Koester & Allard 2000). Determining the location of the red edge in theoretical models is difficult because of convective and nonlinear effects (Brickhill 1983; Bradley & Winget 1994; Wu & Goldreich 1999, 2001). Kanaan et al. (2000a, 2002) conclude that the observed red edge for the ZZ Ceti instability strip at 11,000 K is not an observational selection effect. Finding more DAVs at different temperatures and masses will improve our observational determination of the edges of the ZZ Ceti strip, as well as determine its mass dependence.

Here we list basic data about our observed variables and nonvariables. We will explore the implications of this paper (Paper I) on the shape of the instability strip, its mass dependence, and its purity in Paper II (Mukadam et al. 2004) while taking a closer look at some of the interesting objects found during this search.

3. ARGOS: AN IDEAL CCD PHOTOMETER FOR THE DAV SEARCH

We have designed and placed into operation a CCD camera system optimized for high-speed time series measurements of oscillating white dwarf stars (Nather & Mukadam 2004), which we have named Argos. Our practical limit using the photomultiplier tube (PMT) photometers on the 2.1 m telescope was about magnitude 17.0. We now obtain light curves of comparable quality at magnitude 19.4, a gain of about a factor of 9 in overall sensitivity, essential to observe many of the fainter ZZ Ceti candidates. After light reflects from the primary mirror, it focuses directly onto the small CCD chip without any intervening optics; lack of multiple reflections makes the instrument highly efficient.

We acquire an image scale of 3.05 pixels arcsec^{-1} for our 512×512 pixel CCD chip and a field of view of $2\farcm8$ on a side. Frame transfer, initiated by pulses from a Global Positioning System, allows us to obtain contiguous exposures, which can be as short as 1 s. The CCD is back-illuminated for improved blue sensitivity and provides a quantum efficiency of 80% in the wavelength range 4500–6500 Å, dropping to 30% at 3500 Å. With thermoelectric cooling, we maintain the chip at a temperature of -45°C and obtain a dark current of 1–2 ADU s^{-1} pixel^{-1}. The readout time for the entire chip with no binning is 0.28 s; the readout noise is less than 8 electrons rms. The combination of an efficient instrument and a large amount of telescope time ($\simeq$100 nights yr^{-1}) at the 2.1 m telescope gives us a unique opportunity to search for many pulsators.

4. SELECTION OF DAV CANDIDATES

4.1. *Candidate Databases*

In order to find a substantial number of ZZ Ceti stars, we required a large homogeneous database for candidate selection; we decided to turn to the ongoing Sloan Digital Sky Survey (SDSS) and the Hamburg Quasar Survey (HQS).

4.1.1. *Sloan Digital Sky Survey*

Using a dedicated 2.5 m telescope with a CCD camera (see Gunn et al. 1998), the SDSS will ultimately result in five-band photometry of 10,000 deg^2 in the north Galactic cap (York et al. 2000). It is a calibrated photometric and astrometric digital survey (see Hogg et al. 2001; Pier et al. 2003) with follow-up spectroscopy of selected objects, mainly targeting bright galaxies and quasars from the imaging survey. Potential white dwarfs are allocated fibers for spectroscopy only when the number of targets is insufficient to fill the 640-fiber spectroscopic plug plates (Kleinman et al. 2004). There have been two public data releases by the SDSS: the Early Data Release (EDR; Stoughton et al. 2002) and Data Release 1 (DR1; Abazajian et al. 2003). Kleinman et al. (2004) present 2561 spectroscopically identified white dwarfs from DR1; Harris et al. (2003) presented the initial survey of the SDSS white dwarfs.

4.1.2. *Hamburg Quasar Survey*

Hagen et al. (1995) describe the HQS as a wide-angle objective prism survey to find bright quasars in the northern sky in an area of 14,000 deg^2 by using plates taken at the Calar Alto Schmidt telescope. Homeier & Koester (2001a) have produced a catalog of about 3000 DA white dwarfs in the temperature range of 9000–30,000 K using an automated classification of the low-resolution digitized photographic spectra, 1100 of which were found to have effective temperatures close to the ZZ Ceti instability strip. Homeier et al. (1998) present $T_{\rm eff}$ and $\log g$ values from follow-up spectroscopy of 80 HQS DA white dwarfs.

4.2. *Techniques to Select the SDSS DAV Candidates*

We outline below the different techniques that we used to select the SDSS DAV candidates along with the corresponding success rates. The success rate of discovering ZZ Ceti stars depends not only on the number of variables found but also on our definition of a nonvariable, i.e., at what detection threshold do we stop pursuing a DAV candidate and call it a nonvariable. The success rate for all search techniques is higher for brighter stars ($14.5 \leq B \leq 17.5$), for which we obtain a typical noise level of 1–3 mma[11] in 1–1.5 hr runs with Argos on the 2.1 m telescope. However, most of our targets are fainter ($18 \leq B \leq 19.5$) and require a larger amount of telescope time to achieve the same noise level. For such stars, our typical 2 hr observing runs lead to a detection threshold of 3–6 mma with Argos.

4.2.1. *Photometric Technique for the SDSS DAV Candidates*

Greenstein (1982) acquired multichannel spectrophotometry for 14 DAVs and found that they lie in a narrow range in color space $-0.41 \leq G-R \leq -0.29$. He concluded that the narrowband ($G-R$) color is an excellent temperature indicator for DAs. The SDSS color system comprising the filters u, g, r, i, and z, calibrated by Smith et al. (2002), is a broadband color system like that of Johnson. Fontaine et al. (1982) show that DAV candidate selection based on the Johnson filter system

[11] One millimodulation amplitude (mma) corresponds to 0.1% change in intensity.

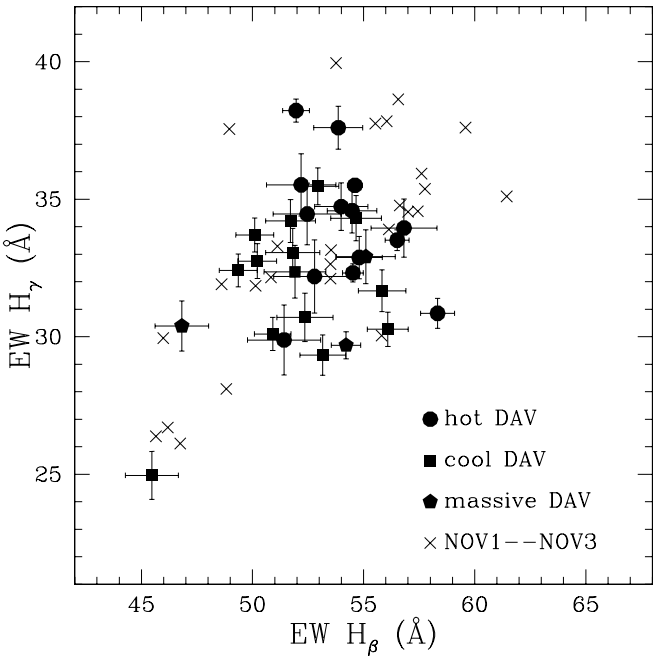

FIG. 1.—Plot of equivalent widths of Hγ and Hβ lines for the observed SDSS DA white dwarfs: all but one of the SDSS pulsators are localized, and in this region we find a success rate of 56% at a detection threshold of 1–3 mma.

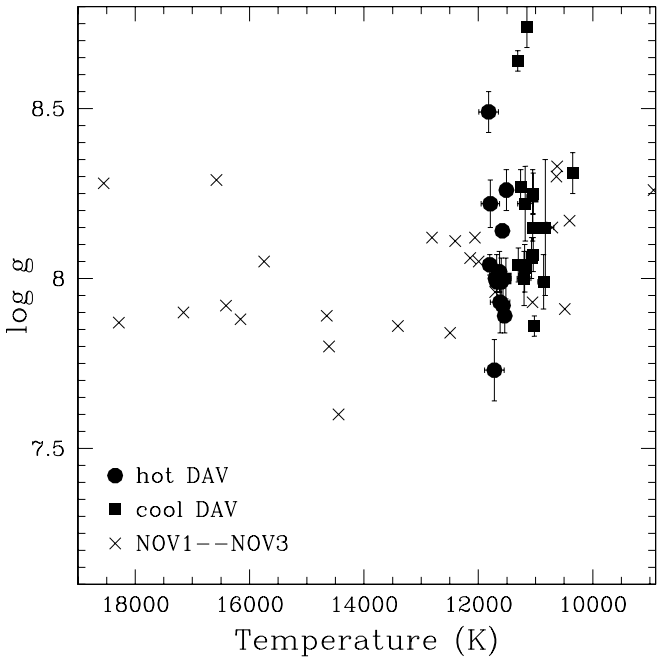

FIG. 2.—Temperature and log g determinations of the observed SDSS DA white dwarfs using Koester's model atmospheres. By restricting our observations in the range $11,000\ \mathrm{K} < T_{\mathrm{eff}} < 12,500\ \mathrm{K}$, we achieve a success rate of 80% in identifying new DAV stars with this method.

yields a 30% success rate for spectroscopically identified DA white dwarfs. Hence, we expected to find one pulsator for every three candidates observed at the telescope and started using the photometric technique in the initial stages of the project.

Selection of candidates from the SDSS EDR (Stoughton et al. 2002) required us to calibrate the DAV strip in the SDSS colors as the EDR did not include any known DAVs. The original SDSS filter system u', g', r', i', and z' is described in Fukugita et al. (1996). Stoughton et al. (2002) describe how the current adaptation u, g, r, i, and z differs from the original filters. We utilized this technique in the early stages of the search, and hence the following description alone is given in terms of the original SDSS filter system.

Lenz et al. (1998) derived synthetic colors in the SDSS filter system for white dwarfs with multichannel spectrophotometric (MCSP) data from Greenstein & Liebert (1990). We used DA white dwarfs common to both papers and compared their MCSP $G-R$ colors with their synthetic SDSS $g'-r'$ colors and also $U-V$ colors with $u'-g'$ colors. By neglecting higher order terms, a best-fit parabola to the resultant plots gave us the following transformations:

$$g' - r' = a + b(G - R) + c(G - R)^2, \quad (1)$$

$$u' - g' = d + e(U - V) + f(U - V)^2, \quad (2)$$

where $a = 0.0296 \pm 0.0057$, $b = 0.679 \pm 0.010$, $c = 0.000 \pm 0.024$, $d = 0.137 \pm 0.011$, $e = 0.776 \pm 0.029$, and $f = 0.013 \pm 0.021$.

With our semitheoretical transformation in hand, we chose spectroscopically identified DA white dwarfs in the color range $0.3 \leq u'-g' \leq 0.6$ and $-0.26 \leq g'-r' \leq -0.16$ as our highest priority candidates. We achieved a success rate of 25% at the detection threshold of 1–3 mma for the candidates so chosen. We found the success rate to be 13% for the detection threshold of 3–6 mma. We found five pulsators with this technique (Mukadam et al. 2003a) before moving to spectroscopic selection techniques with a higher yield.

4.2.2. *Equivalent Width Technique for the SDSS DAV Candidates*

Although the primary goal of the SDSS is extragalactic objects, spectroscopy of interesting stellar objects is also obtained. The SDSS program to target quasars and other blue objects resulted in many white dwarf spectra. DA white dwarf spectra show Balmer absorption lines, pressure broadened by the extremely high gravity. The SDSS spectra cover a wavelength range of 3800–9200 Å and have a resolving power of $\sim$2000, sufficient to resolve the absorption lines clearly. The equivalent widths of the Hβ and Hγ lines correlate well with the effective temperature of the star, which essentially determines whether or not the star will pulsate.

We have measured the equivalent widths of the Hβ and Hγ lines for all the observed variables and nonvariables, which had been previously selected by the photometric method. We find that the variables form a cluster in equivalent width space (except for the unusual pulsator WD 2350−0054), as shown in Figure 1, suggesting a new technique to preselect ZZ Ceti candidates. It is not necessary to derive the absolute temperature of a DAV candidate for this relative method but to compare its equivalent widths (for Hβ and Hγ) with those from a homogeneous set of observed variables and nonvariables. We find a success rate of 30% at the detection threshold of 3–6 mma and a success rate of 56% at the detection threshold of 1–3 mma for this technique. This is effectively a low-resolution spectroscopic technique and hence has a lower success rate compared with the following spectroscopic technique. Except for the opacity maximum, there are generally two temperature solutions for a given equivalent width of Hβ and Hγ (see Fig. 4 in Bergeron et al.

TABLE 1

NEW ZZ CETI VARIABLES

Object	SDSS Object Name	Plate	MJD	Fiber	R.A. (J2000)	Decl. (J2000)	$T_{\rm eff}$ (K)	$\log g$	EW(Hβ) (Å)	EW(Hγ) (Å)	$u-g$	$g-r$	g
WD 0102−0032[a]	SDSS J010207.17−003259.4	396	51816	262	01 02 07	−00 32 59	11050 ± 100	8.24 ± 0.08	54.66 ± 1.14	34.31 ± 0.82	0.43	−0.04	18.21
WD 0111+0018	SDSS J011100.63+001807.2	694	52209	597	01 11 01	+00 18 07	11510 ± 110	8.26 ± 0.06	52.19 ± 1.56	35.52 ± 1.13	0.41	−0.19	18.76
WD 0214−0823	SDSS J021406.78−082318.4	668	52162	354	02 14 07	−08 23 18	11570 ± 090	7.92 ± 0.05	54.80 ± 1.04	32.88 ± 0.77	0.28	−0.14	17.92
WD 0318+0030[a, b]	SDSS J031847.09+003029.9	413	51821	483	03 18 47	+00 30 30	11040 ± 070	8.07 ± 0.05	56.09 ± 0.92	30.27 ± 0.62	0.44	−0.18	17.81
WD 0332−0049[a]	SDSS J033236.61−004918.3	415	51810	211	03 32 37	−00 49 18	11040 ± 070	8.25 ± 0.06	53.16 ± 1.03	29.33 ± 0.73	0.42	−0.11	18.18
WD 0815+4437	SDSS J081531.75+443710.3	547	51959	350	08 15 32	+44 37 10	11620 ± 170	7.93 ± 0.09	52.79 ± 1.83	32.19 ± 1.33	0.34	−0.06	19.30
WD 0825+4119	SDSS J082547.00+411900.0	760	52264	604	08 25 47	+41 19 00	11820 ± 170	8.49 ± 0.06	55.10 ± 1.33	32.91 ± 0.98	0.34	−0.11	18.50
WD 0842+3707	SDSS J084220.73+370701.7	864	52320	548	08 42 21	+37 07 02	11720 ± 170	7.73 ± 0.09	56.82 ± 1.48	33.95 ± 1.06	0.54	−0.18	18.75
WD 0847+4510	SDSS J084746.81+451006.3	763	52235	144	08 47 47	+45 10 06	11680 ± 110	8.00 ± 0.07	53.99 ± 1.20	34.73 ± 0.86	0.42	−0.22	18.32
WD 0906−0024[a]	SDSS J090624.26−002428.2	470	51929	081	09 06 24	−00 24 28	11520 ± 090	8.00 ± 0.06	52.94 ± 0.95	35.47 ± 0.67	0.44	−0.18	17.73
WD 0923+0120	SDSS J092329.81+012020.0	473	51929	074	09 23 29	+01 20 20	11150 ± 70	8.74 ± 0.06	46.82 ± 1.20	30.39 ± 0.91	0.29	−0.16	18.34
WD 0939+5609	SDSS J093944.89+560940.2	556	51991	476	09 39 45	+56 09 40	11790 ± 160	8.22 ± 0.07	52.46 ± 1.53	34.46 ± 1.12	0.43	−0.17	18.70
WD 0942+5733[a]	SDSS J094213.13+573342.5	452	51911	023	09 42 13	+57 33 43	11260 ± 070	8.27 ± 0.05	50.91 ± 0.82	30.10 ± 0.60	0.39	−0.13	17.43
WD 0949−0000[b]	SDSS J094917.04−000023.6	266	51630	037	09 49 17	−00 00 24	11180 ± 130	8.22 ± 0.11	51.42 ± 1.65	29.88 ± 1.27	0.45	−0.13	18.80
WD 0958+0130	SDSS J095833.13+013049.3	500	51994	163	09 58 33	+01 30 49	11680 ± 060	7.99 ± 0.03	51.96 ± 0.60	38.22 ± 0.42	0.41	−0.23	16.70
WD 1015+0306	SDSS J101548.01+030648.4	503	51999	329	10 15 48	+03 06 48	11580 ± 030	8.14 ± 0.02	54.61 ± 0.34	35.50 ± 0.24	0.37	−0.10	15.66
WD 1015+5954	SDSS J101519.65+595430.5	559	52316	330	10 15 20	+59 54 31	11630 ± 110	8.02 ± 0.06	54.48 ± 1.11	34.58 ± 0.81	0.65	−0.31	17.95
WD 1056−0006[a]	SDSS J105612.32−000621.7	276	51909	073	10 56 12	−00 06 22	11020 ± 050	7.86 ± 0.03	49.36 ± 0.85	32.41 ± 0.60	0.15	−0.20	17.52
WD 1122+0358[a]	SDSS J112221.10+035822.4	836	52376	214	11 22 21	+03 58 22	11070 ± 080	8.06 ± 0.06	51.71 ± 1.12	34.21 ± 0.78	0.47	−0.01	18.13
WD 1125+0345	SDSS J112542.84+034506.3	836	52376	050	11 25 43	+03 45 06	11600 ± 120	7.99 ± 0.07	53.86 ± 1.10	37.60 ± 0.78	0.46	−0.12	18.07
WD 1157+0553	SDSS J115707.43+055303.6	841	52375	377	11 57 07	+05 53 04	11050 ± 050	8.15 ± 0.04	50.22 ± 0.87	32.75 ± 0.63	0.32	−0.04	17.59
WD 1345−0055	SDSS J134550.93−005536.5	300	51666	288	13 45 51	−00 55 37	11800 ± 060	8.04 ± 0.03	56.51 ± 0.54	33.51 ± 0.38	0.38	−0.17	16.70
WD 1354+0108	SDSS J135459.89+010819.3	301	51641	322	13 55 00	+01 08 19	11700 ± 050	8.00 ± 0.02	54.52 ± 0.47	32.32 ± 0.33	0.42	−0.17	16.36
WD 1417+0058[a]	SDSS J141708.81+005827.2	304	51609	345	14 17 09	+ 00 58 27	11300 ± 080	8.04 ± 0.05	55.83 ± 1.07	31.67 ± 0.76	0.47	−0.22	18.03
WD 1443+0134[c]	SDSS J144330.93+013405.8	537	52027	279	14 43 31	+01 34 06	10830 ± 150	8.15 ± 0.20	...	...	0.46	−0.12	18.72
WD 1502−0001[a]	SDSS J150207.02−000147.1	310	51990	229	15 02 07	−00 01 47	11200 ± 120	8.00 ± 0.08	52.36 ± 1.26	30.70 ± 0.88	0.37	−0.14	18.68
WD 1524−0030[a, d]	SDSS J152403.25−003022.9	...	...	...	15 24 03	−00 30 23	...	...	...	...	0.38	−0.23	16.03
WD 1617+4324[a]	SDSS J161737.63+432443.8	815	52374	390	16 17 38	+43 24 44	11190 ± 100	8.03 ± 0.07	51.81 ± 1.22	33.06 ± 0.88	0.45	−0.19	18.33
WD 1700+3549[a]	SDSS J170055.38+354951.1	820	52433	110	17 00 55	+35 49 51	11160 ± 050	8.04 ± 0.04	50.10 ± 0.85	33.70 ± 0.62	0.47	−0.16	17.26
WD 1711+6541	SDSS J171113.01+654158.3	350	51691	362	17 11 13	+ 65 41 58	11310 ± 040	8.64 ± 0.03	54.32 ± 0.63	28.54 ± 0.46	0.19	−0.11	16.89
WD 1724+5835[b]	SDSS J172428.42+583539.0	366	52017	264	17 24 28	+58 35 39	11540 ± 080	7.89 ± 0.05	58.33 ± 0.77	30.85 ± 0.54	0.43	−0.19	17.54
WD 1732+5905[b]	SDSS J173235.19+590533.4	366	52017	591	17 32 35	+59 05 33	10860 ± 100	7.99 ± 0.08	51.91 ± 1.39	32.36 ± 0.96	0.47	−0.10	18.74
WD 2350−0054	SDSS J235040.72−005430.9	386	51788	135	23 50 41	−00 54 31	10350 ± 060	8.31 ± 0.06	45.81 ± 1.23	27.16 ± 0.90	0.42	−0.11	18.10

NOTE.—Units of right ascension are hours, minutes, and seconds, and units of declination are degrees, arcminutes, and arcseconds. The latest $T_{\rm eff}$ and $\log g$ fits should be obtained either from the SDSS web site directly or from http://www.whitedwarf.org at a future date.

[a] Large pulsation amplitudes in cDAVs imply that the true uncertainty in their photometric magnitudes can be as high as 0.1–0.2.

[b] Multiple spectra: WD 0318+0030 (413 51929 494), WD 0949−0000 (266 51602 31), WD 1724+5835 (356 51779 271), WD 1732+5905 (356 51779 584), WD 1345−0055 (300 51943 282), WD 1354+0108 (301 51942 324), and WD 1417+0058 (304 51957 338).

[c] The SDSS spectrum of WD 1443+0134 shows only half of the Hγ line; its temperature and $\log g$ values are not reliable.

[d] WD 1524−0030 does not have a spectrum; photometric ID information: Run = 756, Rerun = 8, Camcol = 2, and Field ID = 769.

TABLE 2

NOT OBSERVED TO VARY (NOV; MOSTLY SINGLE 2 hr OBSERVING RUNS) AT A DETECTION THRESHOLD OF 1–3 mma

Object	SDSS Object Name	Plate	MJD	Fiber	R.A. (J2000)	Decl. (J2000)	$T_{\rm eff}$ (K)	$\log g$	EW(Hβ) (Å)	EW(Hγ) (Å)	$u-g$	$g-r$	g	NOV (mma)
WD 0040−0021	SDSS J004022.88−002130.1	392	51793	063	00 40 23	−00 21 30	16160 ± 060	7.88 ± 0.01	53.51 ± 0.25	32.64 ± 0.17	0.39	−0.13	14.83	NOV1
WD 0152+0100	SDSS J015259.20+010018.4	402	51793	523	01 52 59	+01 00 18	12490 ± 070	7.84 ± 0.02	59.59 ± 0.47	37.60 ± 0.33	0.53	−0.16	16.43	NOV2
WD 0210+1243	SDSS J021028.69+124319.0	428	51883	138	02 10 29	+12 43 19	17160 ± 090	7.90 ± 0.02	55.81 ± 0.58	30.04 ± 0.36	0.19	−0.37	16.86	NOV3
WD 0222−0100	SDSS J022207.04−010050.3	406	51817	252	02 22 07	−01 00 50	12060 ± 120	8.12 ± 0.05	56.56 ± 1.03	38.63 ± 0.71	0.39	−0.16	18.04	NOV3
WD 0257+0101	SDSS J025746.41+010106.1	410	51816	578	02 57 46	+01 01 06	16580 ± 210	8.29 ± 0.04	57.61 ± 0.86	35.93 ± 0.57	0.16	−0.27	17.66	NOV3
WD 0318+0044	SDSS J031802.34+004439.8	413	51821	466	03 18 02	+00 44 40	18290 ± 240	7.87 ± 0.04	48.82 ± 1.13	28.10 ± 0.74	0.11	−0.29	18.35	NOV3
WD 0733+2831	SDSS J073356.99+283123.8	754	52232	226	07 33 57	+28 31 24	14610 ± 290	7.80 ± 0.06	56.63 ± 1.44	34.77 ± 1.01	0.32	−0.25	18.83	NOV3
WD 0740+2505	SDSS J074033.49+250511.9	857	52314	388	07 40 33	+25 05 12	18560 ± 190	8.28 ± 0.04	53.51 ± 0.93	32.11 ± 0.64	0.13	−0.35	17.83	NOV2
WD 0746+3510	SDSS J074633.01+351022.8	542	51991	476	07 46 33	+35 10 23	...	...	51.12 ± 0.57	33.29 ± 0.40	0.24	−0.30	16.69	NOV2
WD 0747+2503	SDSS J074724.61+250351.1	857	52314	625	07 47 25	+25 03 51	11050 ± 110	7.93 ± 0.08	53.53 ± 1.01	33.15 ± 0.71	0.44	−0.12	18.39	NOV3
WD 0751+4335	SDSS J075115.11+433513.9	434	51885	445	07 51 15	+43 35 14	19330 ± 200	8.11 ± 0.03	48.61 ± 1.23	31.91 ± 0.82	0.12	−0.33	18.38	NOV3
WD 0814+4608	SDSS J081451.28+460803.6	441	51868	280	08 14 51	+46 08 04	14450 ± 230	7.60 ± 0.06	50.83 ± 0.90	32.16 ± 0.62	0.39	−0.20	17.79	NOV2
WD 0827+4224	SDSS J082716.89+422418.7	761	52266	476	08 27 17	+42 24 19	16410 ± 090	7.92 ± 0.02	50.14 ± 0.82	31.85 ± 0.56	0.19	−0.29	17.44	NOV3
WD 0946+5814	SDSS J094624.31+581445.4	453	51915	124	09 46 24	+58 14 45	08940 ± 020	8.26 ± 0.04	27.02 ± 0.89	17.62 ± 0.66	0.48	−0.04	17.39	NOV3
WD 0949−0019	SDSS J094901.28−001909.5	266	51630	026	09 49 01	−00 19 10	10710 ± 030	8.15 ± 0.03	46.75 ± 0.57	26.12 ± 0.43	0.46	−0.16	16.51	NOV3
WD 1136−0136.....	SDSS J113604.01−013658.2	327	52294	535	11 36 04	−01 36 58	11710 ± 070	7.96 ± 0.04	57.00 ± 0.89	34.54 ± 0.63	0.37	−0.19	17.76	NOV2
WD 1138+6239	SDSS J113854.36+623903.4	776	52319	511	11 38 54	+62 39 03	14650 ± 230	7.89 ± 0.05	53.76 ± 1.24	39.95 ± 0.87	0.24	−0.28	18.38	NOV3
WD 1235+5206	SDSS J123541.62+520611.9	885	52379	231	12 35 42	+52 6 12	12140 ± 100	8.06 ± 0.04	57.76 ± 0.63	35.37 ± 0.45	0.41	−0.22	16.87	NOV2
WD 1243+6248	SDSS J124341.27+624836.3	782	52320	360	12 43 41	+62 48 36	11990 ± 130	8.05 ± 0.06	57.44 ± 0.98	34.56 ± 0.71	0.50	−0.22	17.85	NOV3
WD 1302−0050	SDSS J130247.98−005002.7	294	51986	293	13 02 48	−00 50 03	10640 ± 030	8.30 ± 0.02	46.18 ± 0.55	26.70 ± 0.39	0.40	−0.13	16.55	NOV3
WD 1444−0059	SDSS J144433.80−005958.9	308	51662	256	14 44 34	−00 59 59	15750 ± 070	8.05 ± 0.02	56.14 ± 0.45	33.90 ± 0.32	0.36	−0.18	16.22	NOV2
WD 1529+0020[a, b]	SDSS J152933.26+002031.2	314	51641	354	15 29 33	+00 20 31	10490 ± 060	7.91 ± 0.06	48.96 ± 1.04	37.55 ± 0.71	0.48	−0.12	18.21	NOV3
WD 1659+6209	SDSS J165935.59+620934.0	351	51780	372	16 59 36	+62 09 34	12410 ± 080	8.11 ± 0.03	56.04 ± 0.45	37.83 ± 0.33	0.42	−0.19	16.25	NOV2
WD 1659+6352	SDSS J165926.58+635212.9	349	51699	520	16 59 27	+63 52 13	10410 ± 030	8.17 ± 0.03	45.65 ± 0.93	26.38 ± 0.65	0.44	−0.14	17.88	NOV3
WD 1718+5621	SDSS J171857.82+562150.2	367	51997	416	17 18 58	+56 21 50	12810 ± 090	8.12 ± 0.03	55.53 ± 0.73	37.75 ± 0.50	0.38	−0.21	17.47	NOV3
WD 1735+5730	SDSS J173513.30+573011.5	366	52017	053	17 35 13	+57 30 12	13410 ± 160	7.86 ± 0.03	61.44 ± 0.48	35.10 ± 0.33	0.37	−0.25	16.51	NOV2
WD 2326−0023	SDSS J232659.21−002348.0	383	51818	111	23 26 59	−00 23 47	10620 ± 050	8.33 ± 0.04	45.98 ± 0.87	29.95 ± 0.63	0.49	−0.09	17.52	NOV2

NOTE.—Units of right ascension are hours, minutes, and seconds, and units of declination are degrees, arcminutes, and arcseconds.

[a] The star is a member of a DA4M binary system.

[b] The nonvariability limit of 3 mma comes from a half-hour long observing run and must be regarded with prudence.

TABLE 3

NOV AT A DETECTION THRESHOLD ≥4 mma (MOSTLY SINGLE 2 HR OBSERVING RUNS)

Object	SDSS Object Name	Plate	MJD	Fiber	R.A. (J2000)	Decl. (J2000)	$T_{\rm eff}$ (K)	log g	EW(Hβ) (Å)	EW(Hγ) (Å)	$u-g$	$g-r$	g	NOV (mma)
WD 0037+0031	SDSS J003719.13+003139.2	392	51793	531	00 37 19	+00 31 39	10960 ± 050	8.41 ± 0.03	51.11 ± 0.84	30.54 ± 0.61	0.38	−0.07	17.48	NOV5
WD 0050−0023	SDSS J005047.62−002316.9	394	51876	225	00 50 48	−00 23 17	11490 ± 090	8.98 ± 0.03	55.53 ± 1.39	31.15 ± 0.99	0.31	−0.10	18.81	NOV6
WD 0054−0025[a]	SDSS J005457.61−002517.1	394	51812	118	00 54 58	−00 25 17	10100 ± 060	8.02 ± 0.07	50.75 ± 1.37	30.84 ± 0.92	0.32	−0.16	18.55	NOV8
WD 0106−0014[b]	SDSS J010622.99−001456.3	396	51816	068	01 06 23	−00 14 56	14360 ± 210	7.50 ± 0.05	48.98 ± 1.20	35.95 ± 0.83	0.50	−0.22	18.18	NOV9
WD 0135−0057	SDSS J013545.62−005740.1	400	51820	060	01 35 46	−00 57 40	12570 ± 500	7.80 ± 0.10	56.67 ± 1.30	36.91 ± 0.92	0.40	−0.20	18.52	NOV5
WD 0215−0015	SDSS J021553.99−001550.5	703	52209	174	02 15 54	−00 15 51	15820 ± 160	7.85 ± 0.04	51.88 ± 1.42	34.60 ± 0.95	0.21	−0.28	18.65	NOV8
WD 0217+0058	SDSS J021744.29+005823.9	405	51816	601	02 17 44	+00 58 24	13600 ± 240	7.94 ± 0.04	57.35 ± 0.86	38.99 ± 0.58	0.37	−0.22	17.53	NOV7
WD 0224+0038	SDSS J022435.46+003857.5	406	51817	501	02 24 35	+00 38 58	09790 ± 080	8.11 ± 0.12	37.19 ± 1.65	26.94 ± 1.16	0.45	+0.05	19.06	NOV4
WD 0236−0038	SDSS J023613.64−003822.2	407	51820	029	02 36 14	−00 38 22	14280 ± 440	7.65 ± 0.09	56.92 ± 1.68	29.72 ± 1.19	0.44	−0.27	19.25	NOV5
WD 0238+0049	SDSS J023808.09+004908.8	408	51821	420	02 38 08	+00 49 09	13300 ± 300	7.88 ± 0.06	61.18 ± 1.43	38.66 ± 1.00	0.27	−0.19	18.79	NOV5
WD 0303−0808	SDSS J030325.22−080834.9	458	51929	188	03 03 25	−08 08 34	11400 ± 110	8.49 ± 0.06	51.61 ± 1.43	30.33 ± 1.03	0.33	−0.06	18.78	NOV4
WD 0326+0018	SDSS J032619.44+001817.5	414	51869	467	03 26 19	+00 18 18	12150 ± 080	8.09 ± 0.03	60.16 ± 0.76	34.24 ± 0.53	0.38	−0.20	17.42	NOV5
WD 0329−0007	SDSS J032959.57−000732.5	414	51869	037	03 30 00	−00 07 33	16690 ± 330	7.82 ± 0.07	49.62 ± 1.71	29.20 ± 1.18	0.35	−0.21	19.13	NOV7
WD 0330+0024	SDSS J033031.48+002454.9	414	51869	583	03 30 31	+00 24 55	14500 ± 600	7.75 ± 0.09	54.75 ± 1.51	35.38 ± 1.01	0.29	−0.20	18.97	NOV8
WD 0336−0006	SDSS J033648.33−000634.2	415	51810	595	03 36 48	−00 06 34	10400 ± 040	8.26 ± 0.04	44.31 ± 0.95	27.49 ± 0.67	0.39	−0.06	17.93	NOV5
WD 0340+0106	SDSS J034044.10+010621.9	416	51811	420	03 40 44	+01 06 22	12060 ± 140	8.06 ± 0.05	57.95 ± 1.10	40.45 ± 0.76	0.50	−0.17	18.23	NOV5
WD 0345−0036	SDSS J034504.20−003613.5	416	51811	015	03 45 04	−00 36 14	11430 ± 150	7.76 ± 0.09	54.81 ± 1.29	30.30 ± 0.91	0.45	−0.17	19.00	NOV5
WD 0753+3543	SDSS J075328.74+354304.9	757	52238	284	07 53 29	+35 43 05	16620 ± 240	8.28 ± 0.04	53.20 ± 1.30	35.20 ± 0.89	0.11	−0.27	18.46	NOV6
WD 0756+3803	SDSS J075607.77+380331.7	543	52017	550	07 56 08	+38 03 32	16040 ± 250	7.84 ± 0.05	54.61 ± 1.37	34.33 ± 0.95	0.30	−0.29	18.72	NOV5
WD 0816+3307	SDSS J081625.01+330740.4	862	52325	277	08 16 25	+33 07 40	15460 ± 200	7.75 ± 0.05	51.92 ± 0.92	35.19 ± 0.64	0.29	−0.32	17.78	NOV4
WD 0853+0005	SDSS J085325.55+000514.2	468	51912	132	08 53 26	+00 05 14	11750 ± 110	8.11 ± 0.06	56.19 ± 1.14	33.77 ± 0.83	0.39	−0.15	18.23	NOV4
WD 0953−0051	SDSS J095329.20−005100.7	267	51608	099	09 53 29	−00 51 01	10690 ± 100	8.64 ± 0.11	43.13 ± 1.53	25.88 ± 1.10	0.40	−0.05	18.85	NOV4
WD 1019+0000	SDSS J101911.51+000017.3	272	51941	307	10 19 12	+00 00 17	12760 ± 150	8.35 ± 0.06	59.71 ± 1.13	37.16 ± 0.83	0.51	−0.21	18.16	NOV4
WD 1031+6122	SDSS J103116.34+612232.6	772	52375	090	10 31 16	+61 22 33	11480 ± 180	7.68 ± 0.11	52.79 ± 1.46	34.85 ± 1.03	0.57	−0.20	18.71	NOV4
WD 1045−0018[a]	SDSS J104517.79−001833.9	275	51910	230	10 45 18	−00 18 34	09540 ± 040	8.09 ± 0.06	49.30 ± 1.19	30.40 ± 0.81	0.16	−0.14	18.36	NOV4
WD 1103+0037	SDSS J110326.71+003725.9	277	51908	513	11 03 27	+00 37 26	10540 ± 050	8.22 ± 0.05	46.22 ± 0.96	29.22 ± 0.70	0.43	−0.19	17.64	NOV6
WD 1105+0016	SDSS J110515.32+001626.1	277	51908	596	11 05 15	+00 16 26	12850 ± 060	8.26 ± 0.02	59.82 ± 0.29	37.05 ± 0.21	0.35	−0.19	15.20	NOV4
WD 1126+5144	SDSS J112638.75+514430.9	879	52365	472	11 26 39	+51 44 31	11900 ± 150	8.03 ± 0.07	53.61 ± 1.27	34.85 ± 0.91	0.37	−0.19	18.41	NOV4
WD 1216+6158	SDSS J121613.37+615817.0	779	52342	169	12 16 13	+61 58 16	12200 ± 180	8.19 ± 0.07	56.49 ± 1.13	37.49 ± 0.80	0.29	−0.16	18.19	NOV8
WD 1229−0017	SDSS J122959.23−001714.5	289	51990	109	12 29 59	−00 17 15	13160 ± 180	7.89 ± 0.04	58.84 ± 0.78	40.72 ± 0.54	0.45	−0.21	17.36	NOV5
WD 1315−0131	SDSS J131557.18−013125.5	340	51691	587	13 15 57	−01 31 26	12550 ± 210	8.12 ± 0.08	55.85 ± 1.22	35.85 ± 0.89	0.47	−0.21	18.24	NOV4
WD 1337+0104	SDSS J133714.44+010443.8	298	51662	604	13 37 14	+01 04 44	11830 ± 210	8.39 ± 0.11	54.18 ± 1.56	33.14 ± 1.15	0.35	−0.11	18.57	NOV4
WD 1338−0023	SDSS J133831.75−002328.0	298	51662	021	13 38 32	−00 23 27	11650 ± 090	8.08 ± 0.05	54.89 ± 0.68	34.48 ± 0.50	0.45	−0.18	17.09	NOV4
WD 1342−0159	SDSS J134230.14−015932.8	912	52427	590	13 42 30	−01 59 33	11320 ± 160	8.42 ± 0.09	48.05 ± 1.57	34.00 ± 1.14	0.43	−0.15	18.80	NOV4
WD 1345+0328	SDSS J134552.01+032842.6	529	52025	609	13 45 52	+03 28 43	11620 ± 140	7.80 ± 0.08	51.58 ± 1.23	36.92 ± 0.89	0.49	−0.22	18.58	NOV6
WD 1431−0012	SDSS J143154.57−001231.2	306	51637	196	14 31 55	−00 12 31	12200 ± 180	7.92 ± 0.07	57.84 ± 1.22	35.27 ± 0.85	0.45	−0.16	18.40	NOV7
WD 1432+0146	SDSS J143249.11+014615.6	536	52024	318	14 32 49	+01 46 16	11290 ± 070	8.23 ± 0.06	53.62 ± 0.86	33.21 ± 0.63	0.52	−0.16	17.49	NOV5
WD 1443−0006	SDSS J144312.69−000657.9	308	51662	357	14 43 13	−00 06 58	11960 ± 150	7.87 ± 0.07	56.96 ± 1.35	34.07 ± 0.96	0.44	−0.14	18.66	NOV5
WD 1450+5543	SDSS J145040.50+554321.4	792	52353	311	14 50 41	+55 43 21	15010 ± 120	7.48 ± 0.03	49.33 ± 0.83	32.91 ± 0.58	0.31	−0.33	17.21	NOV4

TABLE 3—*Continued*

Object	SDSS Object Name	Plate	MJD	Fiber	R.A. (J2000)	Decl. (J2000)	$T_{\rm eff}$ (K)	log g	EW(Hβ) (Å)	EW(Hγ) (Å)	$u-g$	$g-r$	g	NOV (mma)
WD 1503−0052	SDSS J150330.49−005211.3	310	51990	133	15 03 30	−00 52 11	11600 ± 130	8.21 ± 0.07	55.35 ± 1.12	36.85 ± 0.77	0.43	−0.15	18.39	NOV4
WD 1545+0321	SDSS J154545.35+032150.0	594	52027	500	15 45 45	+03 21 50	15050 ± 370	7.88 ± 0.07	54.82 ± 1.45	37.91 ± 0.98	0.29	−0.24	18.76	NOV4
WD 1642+3824	SDSS J164248.61+382411.2	818	52395	476	16 42 49	+38 24 11	18810 ± 200	8.40 ± 0.04	52.73 ± 1.15	31.70 ± 0.82	0.07	−0.31	17.98	NOV4
WD 1651+6334	SDSS J165128.84+633438.3	349	51699	265	16 51 29	+63 34 38	14190 ± 150	7.68 ± 0.03	54.33 ± 1.09	33.08 ± 0.76	0.38	−0.31	18.21	NOV4
WD 1653+6254	SDSS J165356.29+625451.4	349	51699	208	16 53 56	+62 54 51	13230 ± 170	7.94 ± 0.05	62.35 ± 1.30	39.68 ± 0.91	0.43	−0.21	18.71	NOV8
WD 1657+6244	SDSS J165747.03+624417.5	349	51699	097	16 57 47	+62 44 18	13610 ± 250	7.77 ± 0.05	59.75 ± 1.40	37.82 ± 0.96	0.41	−0.21	18.87	NOV8
WD 1658+3638	SDSS J165815.53+363816.0	820	52433	514	16 58 16	+36 38 16	11110 ± 120	8.36 ± 0.09	50.04 ± 1.85	27.03 ± 1.38	0.43	−0.13	19.15	NOV4
WD 1706+6316	SDSS J170654.01+631659.6	349	51699	030	17 06 54	+63 17 00	13140 ± 100	8.51 ± 0.03	58.84 ± 0.81	32.88 ± 0.58	0.40	−0.13	17.72	NOV4
WD 1718+5909	SDSS J171853.27+590927.5	366	52017	342	17 18 53	+59 09 28	12430 ± 350	7.94 ± 0.11	59.89 ± 1.28	35.29 ± 0.91	0.43	−0.16	18.64	NOV7
WD 1720+6350[a]	SDSS J172045.09+635031.7	350	51691	007	17 20 45	+63 50 32	11690 ± 170	8.08 ± 0.09	50.79 ± 1.34	30.68 ± 0.89	0.28	−0.21	18.63	NOV8
WD 1723+5546[a]	SDSS J172346.69+554619.0	367	51997	512	17 23 47	+55 46 18	11730 ± 120	8.07 ± 0.06	49.54 ± 1.40	38.52 ± 0.96	0.37	−0.14	18.91	NOV5
WD 1724+6205	SDSS J172405.37+620501.4	352	51694	085	17 24 05	+62 05 01	13590 ± 300	7.81 ± 0.06	59.10 ± 1.24	38.11 ± 0.84	0.38	−0.25	18.41	NOV6
WD 1724+6323	SDSS J172452.91+632324.9	352	51694	595	17 24 53	+63 23 25	14530 ± 390	7.79 ± 0.09	52.60 ± 1.59	32.63 ± 1.06	0.31	−0.28	19.01	NOV6
WD 1726+5331	SDSS J172600.16+533104.1	359	51821	178	17 26 00	+53 31 03	11000 ± 110	8.23 ± 0.08	49.55 ± 1.37	27.98 ± 1.01	0.49	−0.14	18.75	NOV7
WD 1735+5356	SDSS J173536.49+535658.1	360	51816	212	17 35 36	+53 56 58	12940 ± 280	7.85 ± 0.07	60.11 ± 1.34	34.77 ± 0.95	0.45	−0.19	18.65	NOV4
WD 2334−0014	SDSS J233454.18−001436.2	384	51821	151	23 34 54	−00 14 36	13370 ± 250	7.86 ± 0.05	56.55 ± 1.28	41.01 ± 0.91	0.41	−0.20	18.33	NOV6
WD 2336−0051	SDSS J233647.01−005114.7	384	51821	008	23 36 47	−00 51 15	13250 ± 250	7.86 ± 0.05	56.61 ± 1.23	40.05 ± 0.88	0.57	−0.25	18.28	NOV5
WD 2341+0032	SDSS J234110.13+003259.9	385	51877	481	23 41 10	+00 33 00	13380 ± 330	7.90 ± 0.08	57.18 ± 1.99	36.38 ± 1.38	0.41	−0.14	19.16	NOV6
WD 2341−0109	SDSS J234141.64−010917.1	385	51877	124	23 41 42	−01 09 17	13090 ± 170	7.92 ± 0.04	58.98 ± 1.07	38.34 ± 0.75	0.47	−0.21	18.04	NOV4
WD 2346−0037	SDSS J234639.77−003716.0	386	51788	297	23 46 40	−00 37 16	12980 ± 330	7.97 ± 0.08	56.63 ± 1.34	36.16 ± 0.95	0.32	−0.20	18.34	NOV6

NOTE.—Units of right ascension are hours, minutes, and seconds, and units of declination are degrees, arcminutes, and arcseconds.

[a] The star is a member of a DAM binary system.

[b] Kleinman et al. (2004) give an interesting discussion of this most probable eclipsing star.

TABLE 4
OBSERVED STARS FROM THE HAMBURG QUASAR SURVEY

Object	Alternate Name	NOV (mma)	R.A. (B1950)	Decl. (B1950)	$T_{\rm eff}$ (K)	B_J
HS 0951+1312.....	...	hDAV	09 51 03.1	+13 12 41	11,000	16.7
HS 0952+1816.....	...	cDAV	09 52 25.4	+18 16 29	11,000	16.2
HS 0406+1700.....	LB 227	NOV1	04 06 37.0	+17 00 03	16,000	15.4
HS 0843+1956.....	WD 0843+199	NOV3	08 43 42.5	+19 56 05	10,000	16.4
HS 0848+1213.....	...	NOV2	08 48 22.0	+12 13 14	13,000	16.6
HS 0914+0424.....	...	NOV2	09 14 18.2	+04 24 08	13,000	16.7
HS 0942+1416.....	...	NOV2	09 42 04.4	+14 16 28	13,000	16.9
HS 0950+0745.....	PG 0950+077	NOV3	09 50 20.4	+07 45 19	12,000	15.6
HS 1102+0032.....	...	NOV2	11 02 41.4	+00 32 37	12,000	14.7
HS 1431+1521.....	PG 1431+153	NOV2	14 31 44.5	+15 21 25	11,000	15.7
HS 1637+1940.....	...	NOV2	16 37 58.9	+19 40 31	12,000	16.7
HS 1643+1423[a].....	PG 1643+143	NOV3	16 43 21.5	+14 23 08	$25{,}450 \pm 260$	15.5
HS 1711+1716.....	...	NOV2	17 11 41.1	+17 16 57	11,000	16.7
HS 2157+8152[b]	...	NOV3	21 57 18.5	+81 53 01	$10{,}700 \pm 40$	$B = 16.0$
HS 2306+1303.....	PG 2306+130	NOV1	23 06 00.3	+13 03 07	13,000	15.2
HS 2322+2040.....	PG 2322+206	NOV1	23 22 05.4	+20 40 04	13,000	15.5
HS 0727+6915[c].....	...	NOV4	07 27 34.6	+69 15 57	$12{,}100 \pm 250$	$B = 16.9$
HS 0827+0334.....	...	NOV8	08 27 38.5	+03 34 51	12,000	16.7
HS 0838+1643.....	...	NOV4	08 38 18.7	+16 43 05	11,000	17.1
HS 0852+1916.....	LB 8888	NOV3	08 52 40.1	+19 16 06	13,000	15.7
HS 0926+0828.....	...	NOV6	09 26 56.8	+08 28 58	12,000	16.5
HS 0932+1731.....	...	NOV4	09 32 05.5	+17 31 37	12,000	16.8
HS 0949+0823.....	...	NOV4	09 49 17.5	+08 23 44	12,000	16.6
HS 1654+1927.....	...	NOV5	16 54 17.0	+19 27 46	11,000	16.2

NOTE.—Units of right ascension are hours, minutes, and seconds, and units of declination are degrees, arcminutes, and arcseconds.
[a] $\log g = 7.79 \pm 0.05$ from Finley et al. (1997).
[b] $\log g = 8.71 \pm 0.08$ from Homeier et al. (1998).
[c] $\log g = 8.29 \pm 0.14$ from Homeier et al. (1998).

1995), and this additionally explains the low success rate of this technique.

4.2.3. *Spectroscopic Technique for the SDSS DAV Candidates*

We use D. Koester's atmosphere models that treat convection with $ML2/\alpha = 0.6$,[12] best described in Finley et al. (1997) and references therein, to derive $T_{\rm eff}$ and $\log g$ fits for DA white dwarf spectra in the range 3870–7000 Å. Kleinman et al. (2004) give an elaborate discussion of the method used to derive the temperatures and gravities for these white dwarfs. Since we are empirically establishing the ZZ Ceti strip, as long as we use a consistent set of models for all candidates, we do not need to worry about any minor discrepancies between different theoretical models.

We choose our high-priority ZZ Ceti candidates between an effective temperature of 12,500 and 11,000 K. We achieve a success rate of 80% at a detection threshold of 1–3 mma for this technique and a success rate of 50% at a detection threshold of 3–6 mma. These rates are reflected in Figure 2. We can achieve a higher success rate of 90% by confining our candidates to the temperature range 12,000–11,000 K, but being mainly interested in finding hDAV stars, we choose to include candidates in the temperature range 12,500–12,000 K in our observations. Our choice of candidates will also help in better establishing the blue edge of the ZZ Ceti strip.

Note that we use the spectroscopic technique in conjunction with the equivalent width method during our search. It is therefore difficult to present meaningful statistics on these two techniques separately. However, we realize that equivalent width information is already contained in the line profiles; the equivalent width method is a low-resolution spectroscopic technique. We concur with Fontaine et al. (2001, 2003) that the spectroscopic technique is the most fruitful way to search for these pulsators.

4.3. *Spectroscopic Technique to Select HQS DAV Candidates*

The spectroscopic technique can be applied to photographic spectra as well and has been used to obtain temperature estimates of DA candidates from the HQS (Homeier & Koester 2001b; Homeier 2001). Because of the significantly lower signal-to-noise ratio of the prism spectra, which also do not show a resolved line profile, we typically find errors in $T_{\rm eff}$ of the order of 1000–2000 K. In some cases, we find solutions on the wrong side of the Balmer line maximum (e.g., PG 1632+153). Also, we estimate that 10%–20% of this sample may not be white dwarfs (Homeier 2003). This collectively explains our low success rate at finding DAVs from this sample and why we focused mainly on the SDSS white

[12] Various parameterizations of the mixing-length theory are used to treat convection in models of ZZ Ceti stars. Böhm & Cassinelli (1971) describe the ML2 version of convection, assuming the ratio of the mixing length (l) to the pressure scale height (H), $\alpha \equiv l/H = 1$. Bergeron et al. (1995) analyzed optical and ultraviolet (UV) spectrophotometric data of ZZ Ceti stars and found that model atmospheres calculated using the ML2 version, assuming $\alpha = 0.6$, provide the best internal consistency between the optical and UV temperature estimates, the observed photometry, the trigonometric parallax measurements, and the gravitational redshift masses.

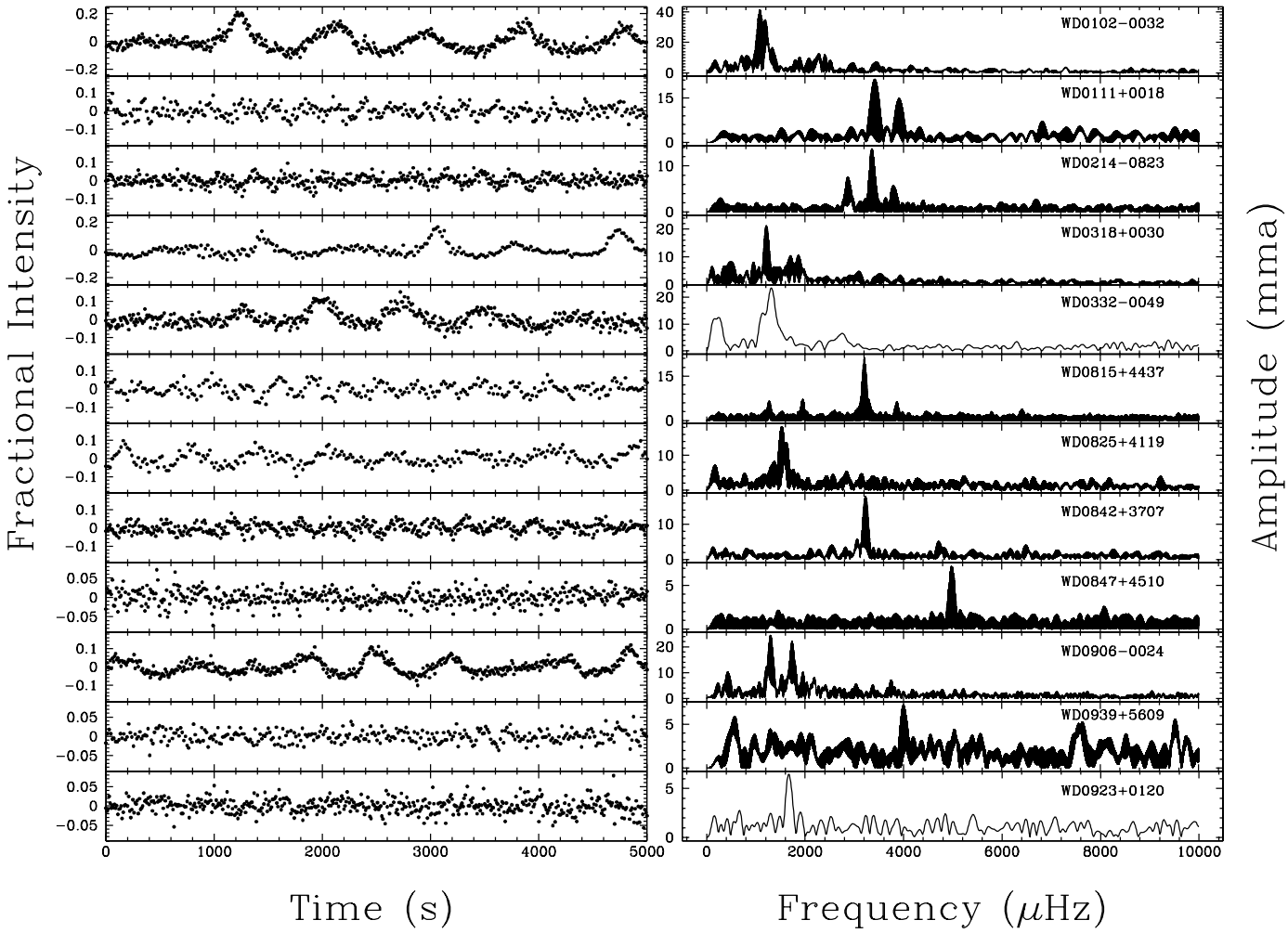

FIG. 3.—Light curves and FTs of the new SDSS DAVs.

dwarfs. We achieve a success rate of 12.5% at the detection threshold of 1–3 mma and 9% for 3–6 mma in finding new DAVs from the HQS.

5. DATA ACQUISITION AND ANALYSIS

5.1. *Observing Strategy*

Searching for coherent signals in light curves helps in overcoming noise, as our signal-to-noise ratio improves with the time base until we reach a limit set by photometric precision. In time series photometry, the signal-to-noise ratio can be calculated in Fourier transform (FT) space. Note that the signal-to-noise ratio depends not only on the magnitude of the star and the amplitude of pulsation modes but also on the quality and duration of the data. We typically observe bright candidates ($14.5 \leq g \leq 17.5$) for 1–1.5 hr each and faint candidates ($18 \leq g \leq 19.5$) for about 2 hr each. We run online data extraction routines that allow us to plot the light curve and FT of the star in real time. If any of these show interesting features, we observe the target for longer. If we find a pulsator, we observe it for a few hours and at least twice to confirm its variability. We have been obtaining multiple 4 hr long data sets on the newly discovered hDAVs for our planet search project.

A ZZ Ceti star may have closely spaced modes or multiplet structure, both of which cause beating effects. A fraction of our low success rate with any technique can be attributed to our single-run investigations of most candidates; an apparent nonpulsator could well be a beating ZZ Ceti star or a low-amplitude variable. Further observations of these stars are interesting to acquire in order to be certain of the purity of the instability strip. We are currently involved in reobserving our apparent nonvariables that lie in our empirically established ZZ Ceti strip.

5.2. *Data Acquisition*

We have obtained high-speed time series photometry with the prime focus CCD photometer Argos on the 2.1 m telescope at McDonald Observatory for 125 nights since 2002 February. During this time, we observed ≈120 SDSS DA white dwarfs and about ≈20 HQS stars. We present our journal of observations for the usable data on the new ZZ Ceti variables in the Appendix in Table 6. We used 5–15 s exposures for most of our targets. We have used a 1 mm thick Schott glass BG40 filter[13] for most of our observations. Pulsation amplitudes are a function of wavelength (Robinson et al. 1995; Nitta et al. 1998, 2000), and we underestimate them by as much as 35%–42% for a DAV in using our CCD (Nather & Mukadam 2004). We use the BG40 filter to suppress the red part of the spectrum and to measure amplitudes

[13] The transmission of this filter can be found at http://www.besoptics.com.

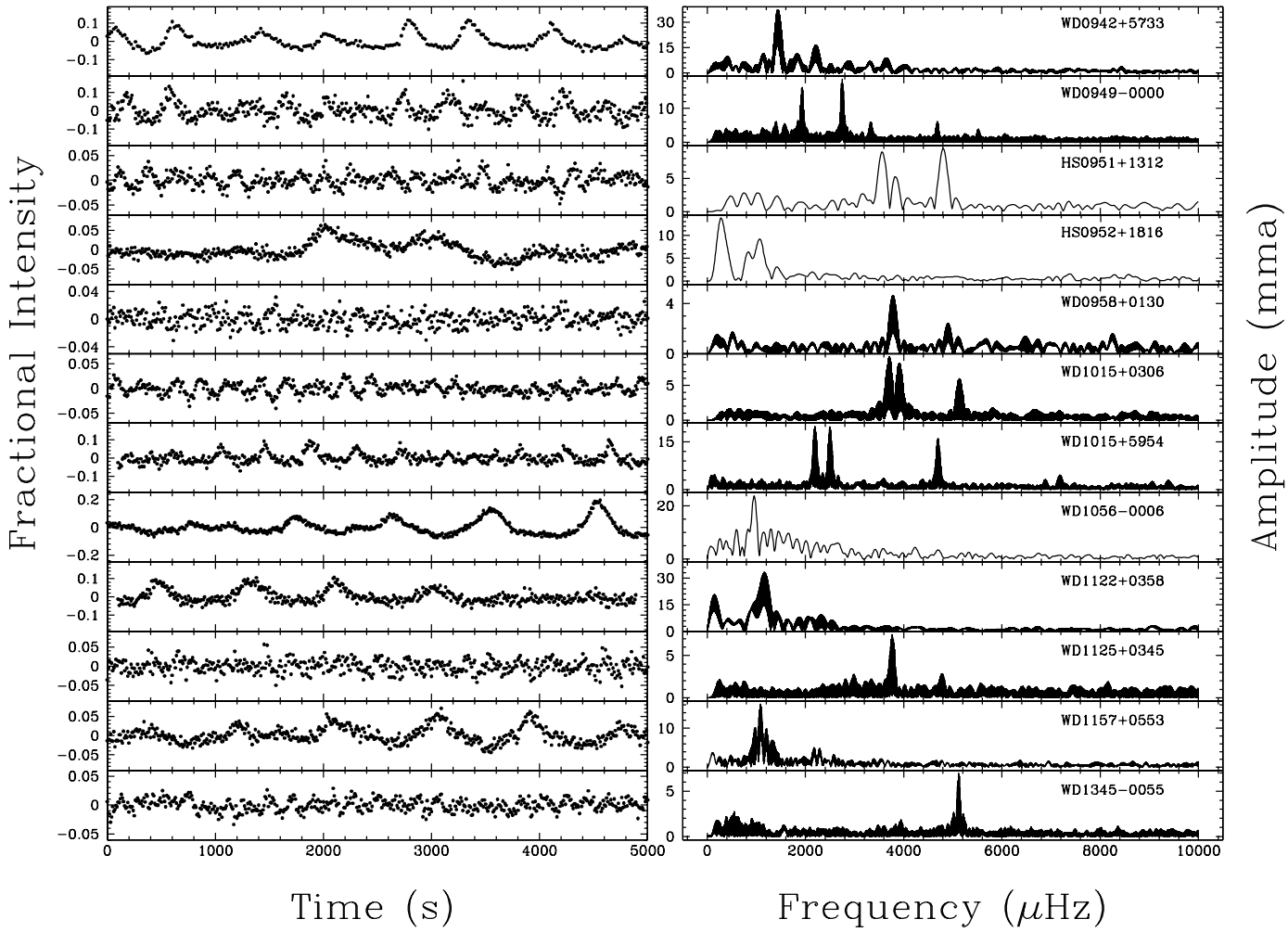

FIG. 4.—Light curves and FTs of the new SDSS DAVs.

comparable to blue-sensitive detectors like PMTs with bialkali photocathodes (see Kanaan et al. 2000b), which have been used to observe variable stars since the late 1960s.

5.3. *Data Reduction and Results*

We extract sky-subtracted light curves from the CCD frames using weighted circular aperture photometry (O'Donoghue et al. 2000). We correct for extinction variations and divide the light curve of the target star with a sum of one or more comparison stars; we prefer brighter stars for the division as their light curves have lower noise. After this preliminary reduction, we bring the data to the same fractional amplitude scale and convert the times of arrival of photons to Barycentric Coordinated Time (TCB; Standish 1998). We then compute a discrete FT for all the light curves.

We present the new DAVs in Table 1, listing their coordinates, temperature and $\log g$ information, colors, equivalent widths, and magnitudes, along with identification numbers required to locate their spectra in the SDSS database. The SDSS spectral objects can be identified on the basis of a plate number, modified Julian date (MJD) of observation, and a fiber number. A single object may have multiple spectra, but the combination of a plate, MJD, and fiber number will always lead to a unique observation. In Tables 2 and 3, we present similar information for our observed nonvariables from the SDSS. The best rereduced photometry and spectral parameters should be obtained from the SDSS directly. We plan to publish and maintain a table with all the pulsators, complete with the latest photometry and spectral fits, at a future date.[14] We list our observed variables and nonvariables with the nonvariability limit, from the HQS in Table 4, some of which are not necessarily DA white dwarfs.

We designate a ZZ Ceti candidate not observed to vary as NOV and add the nonvariability limit as a suffix to this symbol. For example, NOV2 implies a DAV candidate not observed to vary at a detection threshold of 2 mma. If peaks in the FT of a DAV candidate seem to be less than or equal to twice the average amplitude, then these peaks are most probably consistent with noise. The highest white noise peak then defines the detection threshold or the nonvariability limit. If the highest peak is also reflected in the FTs of the reference stars, then we do not use it to define the detection threshold. In that case, we would apply the same test to the second highest peak, and so on. If a peak seems significantly higher than the average amplitude, then we reobserve the candidate to determine whether the peak is real or pure noise. Scargle (1982)

[14] See http://www.whitedwarf.org.

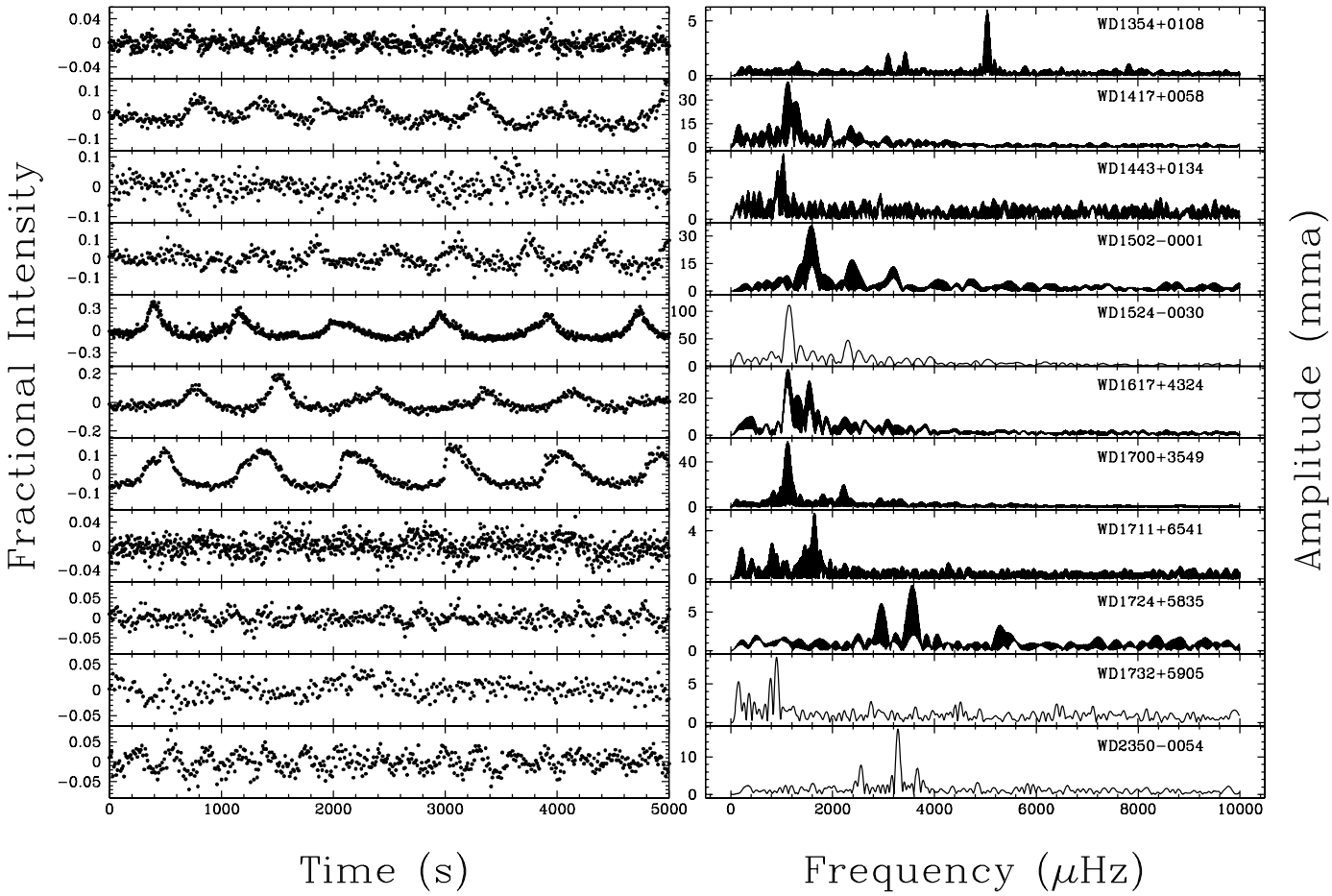

FIG. 5.—Light curves and FTs of the new SDSS DAVs.

gives a thorough discussion of the reliability of detecting a periodic signal in noisy data.

6. PULSATION PROPERTIES OF THE NEW ZZ CETI VARIABLES

We find that the hot DAV stars are mostly distinct from the cool DAV stars in terms of their pulsation characteristics, chiefly the pulsation periods and the pulse shapes. Short pulsation periods typically in the range of 100–300 s are representative of hDAVs, while periods longer than 600 s are typically indicative of cDAVs. Some intermediate-temperature DAVs show a rich pulsation spectrum with periods ranging from a few hundred seconds up to 500 s, exhibiting characteristics of both classes. For our purposes, we classify WD 0111+0018, WD 0214−0823, WD 1015+0306, and WD 1724+5835 as hDAVs since their dominant mode is representative of the hDAV class. We use the same basis to classify WD 0906−0024 as a cDAV. WD 2350−0054 is by far the coolest pulsator and is unusual because it is not expected to pulsate according to our empirical determination of the edges of the ZZ Ceti strip. The effective temperature of WD 2350−0054 derived from its SDSS spectrum places it 650 K below the cool edge of the instability strip. Its spectrum does not show any unusual features that we could attribute to a binary companion or contamination of any sort. Furthermore, it shows pulsation periods and pulse shapes characteristic of the hot DAV stars. The SDSS spectrum of WD 1443+0134 has a missing section, and hence its temperature and $\log g$ values are not reliable.

The hot ZZ Ceti stars show pulse shapes distinct from the cDAVs, e.g., see the light curve of WD 0214−0823 compared with WD 1524−0030. The brighter variables have well-defined pulse shapes, while the low-amplitude faint variables do not. Among the hDAVs, only the light curves of the intermediate-temperature DAVs like WD 1015+5954 show pulse shapes distinct from the rest. The light curves of WD 0923+0120 and WD 1711+6541 show pulse shapes and amplitudes distinct from other cDAVs. Their low amplitude is a result of their high gravity $\log g \geq 8.6$. The nonradial g-modes have a non-negligible radial component, the amplitude of which scales with stellar mass and plays a role in dictating the amplitude of the nonradial component.

We plot the light curves and FTs of all the new variables in Figures 3, 4, and 5. We present the dominant periods of the new variables in Table 5. We choose a resolution of $0.1(1/T)$ to calculate the FTs, where T is the time span of the data. We indicate a column with the resolution of the FT in Table 5 for data on the different pulsators. We also indicate the peak-to-peak amplitude in the light curve in Table 5. In the case of stars that clearly show beating, we choose those sections of the light curve that show the highest peak-to-peak amplitude. We do not have sufficient data on quite a few of the DAVs to discern a multiplet structure if it is present in the pulsation spectrum. Some of the apparent singlets in Table 5 may well

TABLE 5

PULSATION CHARACTERISTICS OF THE NEW ZZ CETI VARIABLES

Object	Period and Amplitude (s, mma)	FT Resolution (μHz)	Peak-to-Peak Amplitude	Preliminary Classification
WD 0102−0032	926.1, 37.2; 830.3, 29.2	1.01	0.28	cDAV
WD 0111+0018.....	292.3, 21.9; 255.3, 15.6	0.19	0.14	hDAV
WD 0214−0823	348.1, 8.5; 347.1, 8.3; 297.5, 16.0; 263.5, 7.1	0.56	0.13	hDAV
WD 0318+0030	826.4, 21.1; 587.1, 10.1; 536.1, 10.6	0.59	0.26	cDAV
WD 0332−0049	767.5, 15.1	11.11	0.21	cDAV
WD 0815+4437	787.5, 6.6; 511.5, 7.3; 311.7, 22.0; 311.3, 9.3; 258.3, 6.2	0.0175	0.16	hDAV
WD 0825+4119	653.4, 17.1; 611.0, 11.2	0.0215	0.18	hDAV
WD 0842+3707	309.3, 17.9	0.55	0.14	hDAV
WD 0847+4510	201.0, 7.3	0.04	0.07	hDAV
WD 0906−0024	769.4, 26.1; 618.8, 9.1; 574.5, 23.7; 457.9, 9.5; 266.6, 7.6	0.37	0.18	cDAV
WD 0923+0120	595.2, 7.4	0.04	11.7	cDAV
WD 0939+5609	249.9, 7.2	0.0181	0.06	hDAV
WD 0942+5733	694.7, 37.7; 550.5, 12.2; 451.0, 18.4	0.0288	0.18	cDAV
WD 0949−0000	711.6, 6.0; 634.2, 5.1; 516.6, 16.2; 365.2, 17.7; 364.0, 7.3; 363.2, 12.5; 213.3, 6.0	0.0557	0.22	cDAV
HS 0951+1312.....	281.6, 8.8; 258.6, 3.6; 208.0, 9.3	17.6	0.07	hDAV
HS 0952+1816.....	1466.0, 4.5; 1159.7, 4.8; 853.8, 3.9	12.9	0.10	cDAV
WD 0958+0130	264.4, 4.7; 203.7, 2.5	0.375	0.05	hDAV
WD 1015+0306	270.0, 8.4; 255.7, 7.3; 194.7, 5.8	0.023	0.06	hDAV
WD 1015+5954	1116.5, 12.6; 453.7, 15.8; 401.7, 20.8; 292.4, 8.5; 213.0, 9.8	0.0223	0.13	hDAV
WD 1056−0006	942.2, 62.3; 474.4, 22.9; 314.2, 11.0	10.7	0.28	cDAV
WD 1122+0358	996.1, 17.9; 859.0, 34.3	0.29	0.13	cDAV
WD 1125+0345	265.8, 3.3; 265.5, 7.2; 208.6, 2.8	0.142	0.08	hDAV
WD 1157+0553	1056.2, 5.8; 918.9, 15.9; 826.2, 8.1; 748.5, 5.6; 458.7, 4.2; 436.1, 3.9	1.10	0.11	cDAV
WD 1345−0055	254.4, 2.4; 195.2, 5.5; 195.5, 3.9	0.144	0.04	hDAV
WD 1354+0108	322.9, 1.9; 291.6, 2.2; 198.3, 6.0; 173.3, 1.1; 127.8, 1.5	0.068	0.05	hDAV
WD 1417+0058	894.5, 44.0; 812.5, 31.5	0.375	0.22	cDAV
WD 1443+0134	1085.0, 5.2; 968.9, 7.5	0.369	0.14	cDAV
WD 1502−0001	687.5, 12.0; 629.5, 32.6; 581.9, 11.1; 418.2, 14.9; 313.6, 13.1	0.381	0.22	cDAV
WD 1524−0030	873.2, 111.5; 434.0, 47.8	14.1	0.54	cDAV
WD 1617+4324	889.6, 36.6; 626.3, 24.1	0.55	0.28	cDAV
WD 1700+3549	955.3, 20.4; 893.4, 54.7; 450.5, 19.3	0.105	0.20	cDAV
WD 1711+6541	1248.2, 3.2; 690.2, 3.3; 606.3, 5.2	0.549	0.06	cDAV
WD 1724+5835	337.9, 5.9; 279.5, 8.3; 189.2, 3.2	0.986	0.07	hDAV
WD 1732+5905	1248.4, 22.5; 1122.4, 10.2	8.32	0.08	cDAV
WD 2350−0054	391.1, 7.5; 304.3, 17.0; 273.3, 6.2	8.69	0.09	cDAV

be multiplets. We do not even have sufficient data on the cDAVs to resolve the closely spaced modes. For some hDAVs with multiplet structure, our single-site data may mislead us to aliases, and hence the periods listed below should be considered preliminary determinations.

7. CONCLUSIONS

We conclude that the spectroscopic technique, determining temperatures and $\log g$ values by comparing the stellar spectra to a grid of atmosphere models, is the most fruitful way to search for ZZ Ceti pulsators, in accordance with Fontaine et al. (2001, 2003). We can achieve a 90% success rate by confining our candidates between 12,000 and 11,000 K with this technique at a detection threshold of 1–3 mma. However, our interest in hDAVs and the blue edge of the instability strip leads us to choose candidates between 12,500 and 11,000 K, reducing our success rate to 80%. With the discovery of 35 new DAVs, we hereby almost double the current sample of 39 published ZZ Ceti stars.

We thank the Texas Advanced Research Program for grant ARP-0543 and NASA for grant NAG5-13094 for funding this project. We also acknowledge NSF for grant AST 98-76730, NASA for grant NAG5-9321, and STScI for grant GO-08254. We thank the AAS for an International Travel Grant for support to attend the Sixth WET Workshop in Naples, where the first author presented this work. We also thank E. L. Robinson and R. Hynes for their support with observing and data reduction algorithms. We thank the referee, Gerard Vauclair, for his helpful comments that made this manuscript a better paper.

Funding for the creation and distribution of the SDSS Archive[15] has been provided by the Alfred P. Sloan Foundation, the Participating Institutions, the National Aeronautics and Space Administration, the National Science Foundation, the US Department of Energy, the Japanese Monbukagakusho, and the Max Planck Society. The SDSS is managed by the Astrophysical Research Consortium (ARC) for the participating institutions. The participating institutions are the University of Chicago, Fermilab, the Institute for Advanced Study, the Japan Participation Group, Johns Hopkins University, Los Alamos National Laboratory, the Max-Planck-Institute for Astronomy (MPIA), the Max-Planck-Institute for Astrophysics (MPA), New Mexico State University, University of Pittsburgh, Princeton University, the United States Naval Observatory, and the University of Washington.

[15] The SDSS Web site is http://www.sdss.org.

APPENDIX

Table 6 is our journal of observations for the usable data on the new ZZ Ceti variables.

TABLE 6
JOURNAL OF OBSERVATIONS FOR USABLE DATA ON NEWLY DISCOVERED DAVS

Run	No. of Images	Target	UTC Start Time	Exposure (s)	Filter
A0105	0794	HS 0952+1816	2002 Feb 07 09:19:43	10	None
A0109	0484	WD 0332−0049	2002 Feb 08 03:03:09	10	None
A0111	1064	WD 0949−0000	2002 Feb 08 05:42:24	10	None
A0112	0825	WD 0949−0000	2002 Feb 08 08:42:05	10	None
A0140	0955	WD 0949−0000	2002 Feb 13 05:32:52	10	None
A0155	1293	WD 0949−0000	2002 Feb 15 06:09:46	10	None
A0183	0239	WD 1056−0006	2002 Apr 11 07:02:46	15	None
A0199	0551	WD 1345−0055	2002 Apr 12 07:40:47	05	BG40
A0209	0316	WD 1056−0006	2002 Apr 17 05:25:27	10	BG40
A0242	0506	WD 1724+5835	2002 Jun 08 03:46:45	10	BG40
A0245	1550	WD 1345−0055	2002 Jun 09 02:46:44	05	BG40
A0247	0510	WD 1724+5835	2002 Jun 09 06:33:08	10	BG40
A0253	0396	WD 1345−0055	2002 Jun 13 06:28:53	10	BG40
A0258	1293	WD 1345−0055	2002 Jun 14 03:04:01	10	BG40
A0262	0403	WD 1345−0055	2002 Jun 15 02:58:08	10	BG40
A0263	0337	WD 1345−0055	2002 Jun 15 04:41:48	10	BG40
A0267	2050	WD 1345−0055	2002 Jun 16 03:04:41	05	BG40
A0274	0572	WD 1345−0055	2002 Jun 17 02:53:57	10	BG40
A0298	0471	WD 1524−0030	2002 Jul 12 04:38:48	10	BG40
A0308	0486	WD 1524−0030	2002 Aug 03 04:17:37	10	BG40
A0312	1479	WD 1524−0030	2002 Aug 04 02:45:36	05	BG40
A0360	0312	WD 1724+5835	2002 Aug 13 06:43:25	10	BG40
A0369	1444	WD 1711+6541	2002 Oct 01 02:08:22	05	BG40
A0376	1146	WD 0102−0032	2002 Oct 02 05:27:35	10	BG40
A0381	2281	WD 1711+6541	2002 Oct 03 01:35:07	05	BG40
A0383	0616	WD 0102−0032	2002 Oct 03 07:18:14	10	BG40
A0396	0842	WD 0332−0049	2002 Oct 29 08:44:58[a]	10	BG40
A0398	0842	WD 1732+5905	2002 Oct 30 01:17:24[a]	10	BG40
A0403	0978	WD 2350−0054	2002 Nov 03 02:33:38[a]	10	BG40
A0405	0901	WD 0332−0049	2002 Nov 03 08:00:44[a]	10	BG40
A0410	1090	WD 2350−0054	2002 Nov 06 03:40:46	10	BG40

TABLE 6—*Continued*

Run	No. of Images	Target	UTC Start Time	Exposure (s)	Filter
A0414	2252	WD 1711+6541	2002 Nov 07 00:52:55	05	BG40
A0415	1152	WD 2350−0054	2002 Nov 07 04:20:25	10	BG40
A0432	0478	WD 0318+0030	2002 Dec 08 06:28:15	20	BG40
A0434	0131	WD 1015+0306	2002 Dec 08 11:13:04	10	BG40
A0436	0861	WD 0318+0030	2002 Dec 10 03:11:31	10	BG40
A0438	0133	WD 0906−0024	2002 Dec 10 07:52:29	15	BG40
A0439	0748	WD 0906−0024	2002 Dec 10 08:46:59	15	BG40
A0440	0310	WD 1015+0306	2002 Dec 10 12:09:16	10	BG40
A0442	0282	WD 0214−0823	2002 Dec 11 03:50:08	15	BG40
A0443	0476	WD 0214−0823	2002 Dec 11 05:02:52	15	BG40
A0446	0877	WD 1015+0306	2002 Dec 11 10:39:54	10	BG40
A0449	0839	WD 0825+4119	2002 Dec 12 09:16:12	10	BG40
A0450	0521	WD 1015+5954	2002 Dec 12 11:42:33	10	BG40
A0452	0741	WD 0214−0823	2002 Dec 13 03:16:55	10	BG40
A0456	0737	WD 0906−0024	2002 Dec 13 08:49:18	10	BG40
A0457	0722	WD 1015+5954	2002 Dec 13 11:00:29	10	BG40
A0467	1122	WD 1354+0108	2003 Jan 26 10:46:34	05	BG40
A0468	0227	WD 1417+0058	2003 Jan 26 12:31:39	10	BG40
A0469	0371	WD 0111+0018	2003 Jan 27 01:30:48	15	BG40
A0474	0122	WD 0214−0823	2003 Jan 28 01:28:47	10	BG40
A0475	0992	WD 0214−0823	2003 Jan 28 01:55:14	10	BG40
A0477	0732	WD 0949−0000	2003 Jan 28 07:09:07	15	BG40
A0480	0702	WD 0815+4437	2003 Jan 29 03:51:05	20	BG40
A0481	1496	WD 1015+0306	2003 Jan 29 08:01:15	05	BG40
A0482	0976	WD 1354+0108	2003 Jan 29 10:27:17	10	BG40
A0499	0299	WD 0111+0018	2003 Feb 02 01:41:23	20	BG40
A0501	0527	WD 1015+5954	2003 Feb 02 06:26:12	20	BG40
A0502	1262	WD 1157+0553	2003 Feb 02 09:34:51	10	BG40
A0506	0541	WD 1157+0553	2003 Feb 03 09:24:12	10	BG40
A0507	0099	WD 1502−0001	2003 Feb 03 11:05:56	15	BG40
A0509	0504	WD 0825+4119	2003 Feb 04 04:39:49	20	BG40
A0513	0487	WD 0847+4510	2003 Feb 05 04:41:02	15	BG40
A0532	0938	WD 1056−0006	2003 Feb 25 08:56:15	10	BG40
A0533	0405	WD 1502−0001	2003 Feb 25 11:41:10	10	BG40
A0534	0504	WD 0847+4510	2003 Feb 26 01:39:46	15	BG40
A0535	0859	WD 0942+5733	2003 Feb 26 03:53:13	10	BG40
A0536	0652	WD 1125+0345	2003 Feb 26 06:25:51	10	BG40
A0541	0653	WD 0939+5609	2003 Feb 27 05:28:49	10	BG40
A0542	0399	WD 0949−0000	2003 Feb 27 07:26:31	10	BG40
A0544	0769	WD 1417+0058	2003 Feb 27 10:39:29	10	BG40
A0545	0828	WD 0842+3707	2003 Feb 28 01:55:37	10	BG40
A0546	1531	WD 0949−0000	2003 Feb 28 04:22:31	10	BG40
A0548	0584	WD 1502−0001	2003 Feb 28 10:58:12	10	BG40
A0550	1535	WD 0949−0000	2003 Mar 01 03:10:10	10	BG40
A0551	1002	WD 1125+0345	2003 Mar 01 07:33:39	10	BG40
A0553	0895	WD 0842+3707	2003 Mar 02 01:58:27	10	BG40
A0554	1281	WD 0949−0000	2003 Mar 02 04:35:41	10	BG40
A0556	0806	WD 1417+0058	2003 Mar 02 10:30:02	10	BG40
A0559	1296	WD 1354+0108	2003 Mar 04 10:55:16	05	BG40
A0560	0751	WD 0847+4510	2003 Mar 05 01:43:09	10	BG40
A0561	0821	WD 0949−0000	2003 Mar 05 03:57:08	10	BG40
A0562	0647	WD 0949−0000	2003 Mar 05 06:19:30	10	BG40
A0563	0810	WD 1125+0345	2003 Mar 05 08:14:59	10	BG40
A0565	0978	WD 0847+4510	2003 Mar 06 01:53:15	10	BG40
A0566	0870	WD 0949−0000	2003 Mar 06 04:42:54	10	BG40
A0567	0914	WD 1125+0345	2003 Mar 06 07:13:30	10	BG40
A0568	1385	WD 1354+0108	2003 Mar 06 09:53:23	05	BG40
A0569	0252	WD 1354+0108	2003 Mar 06 12:17:06	05	BG40
A0572	1481	WD 1354+0108	2003 Mar 22 05:37:39	05	BG40
A0573	0157	WD 1354+0108	2003 Mar 22 07:50:54	05	BG40
A0574	1337	WD 1354+0108	2003 Mar 22 10:30:44	05	BG40
A0575	0331	WD 0815+4437	2003 Mar 23 01:57:17	15	BG40
A0577	4952	WD 1354+0108	2003 Mar 23 05:35:12	05	BG40
A0578	1010	WD 0815+4437	2003 Mar 24 02:00:26	10	BG40
A0580	1944	WD 1354+0108	2003 Mar 24 06:59:51	05	BG40

TABLE 6—*Continued*

Run	No. of Images	Target	UTC Start Time	Exposure (s)	Filter
A0581	0885	WD 1617+4324	2003 Mar 24 09:53:31	10	BG40
A0583	0742	WD 0815+4437	2003 Mar 25 02:08:27	10	BG40
A0584	0390	WD 0939+5609	2003 Mar 25 04:19:52	15	BG40
A0585	0778	HS 0952+1816	2003 Mar 25 06:10:13	10	BG40
A0587	0703	WD 1700+3549	2003 Mar 25 10:20:28	10	BG40
A0590	0320	WD 1617+4324	2003 Mar 26 11:23:52	10	BG40
A0591	0847	WD 0949−0000	2003 Mar 27 02:03:35	10	BG40
A0592	0598	WD 0958+0130	2003 Mar 27 04:55:26	10	BG40
A0593	0543	WD 1122+0358	2003 Mar 27 06:46:11	10	BG40
A0595	0336	WD 0815+4437	2003 Mar 30 02:00:46	10	BG40
A0597	1450	WD 0958+0130	2003 Mar 30 04:56:35	05	BG40
A0598	2063	WD 1354+0108	2003 Mar 30 07:06:26	05	BG40
A0599	0736	WD 1700+3549	2003 Mar 30 10:06:50	10	BG40
A0600	1467	WD 0949−0000	2003 Mar 31 02:02:38	10	BG40
A0601	0974	WD 1122+0358	2003 Mar 31 06:16:02	05	BG40
A0603	1592	WD 0815+4437	2003 Apr 01 01:58:45	10	BG40
A0604	1154	WD 1354+0108	2003 Apr 01 06:31:22	05	BG40
A0605	1354	WD 1443+0134	2003 Apr 01 08:15:39	10	BG40
A0606	1074	WD 0949−0000	2003 Apr 02 02:02:14	10	BG40
A0608	1138	WD 1443+0134	2003 Apr 02 07:25:36	10	BG40
A0609	0250	WD 1443+0134	2003 Apr 03 11:18:15	10	BG40
A0611	0459	WD 1443+0134	2003 Apr 04 09:52:52	15	BG40
A0612	0546	WD 0815+4437	2003 Apr 05 01:57:36	10	BG40
A0613	1237	WD 0923+0120	2003 Apr 05 03:41:48	10	BG40
A0615	1033	WD 1700+3549	2003 Apr 05 09:23:59	10	BG40
A0616	0622	WD 0923+0120	2003 Apr 06 02:02:32	10	BG40
A0618	1568	WD 0949−0000	2003 Apr 07 02:02:15	10	BG40
A0619	0450	WD 0942+5733	2003 Apr 07 06:32:14	20	BG40
A0622	0565	WD 1354+0108	2003 Apr 08 05:43:59	05	BG40
A0625	1046	WD 1015+5954	2003 May 01 02:33:10	10	BG40
A0628	0671	WD 0939+5609	2003 May 02 02:27:38	15	BG40
A0629	2044	WD 1354+0108	2003 May 02 05:24:59	05	BG40
A0631	2204	WD 1345−0055	2003 May 03 03:03:00	10	BG40
A0633	0842	WD 1015+5954	2003 May 04 02:36:30	10	BG40
A0634	0442	WD 1015+5954	2003 May 04 05:53:06	10	BG40
A0639	0107	WD 1354+0108	2003 May 07 04:55:52	05	BG40
A0640	2071	WD 1354+0108	2003 May 07 05:06:52	05	BG40
A0642	1455	WD 1015+5954	2003 May 08 02:57:56	10	BG40
A0643	1016	WD 1354+0108	2003 May 08 07:10:43	10	BG40
A0645	1081	WD 1015+5954	2003 May 09 02:34:36	10	None
A0646	1229	WD 1345−0055	2003 May 09 06:04:12	10	None
A0648	2025	WD 1345−0055	2003 May 10 03:02:25	10	None
A0650	0713	HS 0951+1312	2003 May 11 03:27:23	10	None
A0651	0513	WD 1345−0055	2003 May 11 05:40:19	10	None
A0653	0462	WD 1345−0055	2003 May 12 06:12:26	10	None
A0654	0382	WD 1345−0055	2003 May 12 07:32:21	10	None
A0808	0853	WD 0923+0120	2003 Dec 25 10:02:11	10	BG40

[a] The absolute time of the run is uncertain to within 1 minute. We acquired the data with an undisciplined PC clock by mistake. The relative times between the images, i.e., the exposures, are correct.

REFERENCES

Abazajian, K., et al. 2003, AJ, 126, 2081
Bergeron, P., Fontaine, G., Billères, M., Boudreault, S., & Green, E. M. 2004, ApJ, 600, 404
Bergeron, P., Wesemael, F., Lamontagne, R., Fontaine, G., Saffer, R. A., & Allard, N. F. 1995, ApJ, 449, 258
Böhm, K. H., & Cassinelli, J. 1971, A&A, 12, 21
Bradley, P. A. 2001, ApJ, 552, 326
Bradley, P. A., & Winget, D. E. 1994, ApJ, 421, 236
Brickhill, A. J. 1983, MNRAS, 204, 537
Clemens, J. C. 1993, Ph.D. thesis, Univ. Texas at Austin
Duncan, M. J., & Lissauer, J. J. 1998, Icarus, 134, 303
Finley, D. S., Koester, D., & Basri, G. 1997, ApJ, 488, 375
Fleming, T. A., Liebert, J., & Green, R. F. 1986, ApJ, 308, 176
Fontaine, G., Bergeron, P., Billères, M., & Charpinet, S. 2003, ApJ, 591, 1184
Fontaine, G., Bergeron, P., Brassard, P., Billères, M., & Charpinet, S. 2001, ApJ, 557, 792
Fontaine, G., Bergeron, P., Lacombe, P., Lamontagne, R., & Talon, A. 1985, AJ, 90, 1094
Fontaine, G., Lacombe, P., McGraw, J. T., Dearborn, D. S. P., & Gustafson, J. 1982, ApJ, 258, 651
Fukugita, M., Ichikawa, T., Gunn, J. E., Doi, M., Shimasaku, K., & Schneider, D. P. 1996, AJ, 111, 1748
Giovannini, O., Kepler, S. O., Kanaan, A., Wood, A., Claver, C. F., & Koester, D. 1998, Baltic Astron., 7, 131
Greenstein, J. L. 1982, ApJ, 258, 661
Greenstein, J. L., & Liebert, J. W. 1990, ApJ, 360, 662
Gunn, J. E., et al. 1998, AJ, 116, 3040
Hagen, H.-J., Groote, D., Engels, D., & Reimers, D. 1995, A&AS, 111, 195

Hansen, B. M. S., et al. 2002, ApJ, 574, L155
Harris, H. C., et al. 2003, AJ, 126, 1023
Hogg, D. W., Finkbeiner, D. P., Schlegel, D. J., & Gunn, J. E. 2001, AJ, 122, 2129
Homeier, D. 2001, Ph.D. thesis, Christian-Albrechts-Univ. zu Kiel
———. 2003, in Proc. NATO Advanced Research Workshop on White Dwarfs, ed. D. De Martino (Dordrecht: Kluwer), 371
Homeier, D., & Koester, D. 2001a, Astron. Gesellschaft Abst. Ser., 18, 111
———. 2001b, in ASP Conf. Ser. 226, 12th European Conf. on White Dwarf Stars, ed. H. L. Shipman et al. (San Francisco: ASP), 397
Homeier, D., Koester, D., Hagen, H.-J., Jordan, S., Heber, U., Engels, D., Reimers, D., & Dreizler, S. 1998, A&A, 338, 563
Isern, J., García-Berro, E., Hernanz, M., & Chabrier, G. 2000, ApJ, 528, 397
Isern, J., García-Berro, E., & Salaris, M. 2002, in GAIA: A European Space Project, ed. O. Bienaymé & C. Turon (Les Ulis: EDP Sciences), 123
Kanaan, A., Kepler, S. O., & Winget, D. E. 2002, A&A, 389, 896
Kanaan, A., O'Donoghue, D., Kleinman, S. J., Krzesinski, J., Koester, D., & Dreizler, S. 2000b, Baltic Astron., 9, 387
Kanaan, A., Winget, D. E., Kepler, S. O., & Montgomery, M. H. 2000a, in IAU Colloq. 176, The Impact of Large-Scale Surveys on Pulsating Star Research, ed. L. Szabados & D. W. Kurtz (ASP Conf. Ser. 203; San Francisco: ASP), 518
Kepler, S. O., Mukadam, A., Winget, D. E., Nather, R. E., Metcalfe, T. S., Reed, M. D., Kawaler, S. D., & Bradley, P. A. 2000, ApJ, 534, L185
Kepler, S. O., et al. 1991, ApJ, 378, L45
Kleinman, S. J., et al. 1998, ApJ, 495, 424
———. 2004, ApJ, in press
Koester, D., & Allard, N. F. 2000, Baltic Astron., 9, 119
Lenz, D. D., Newberg, J., Rosner, R., Richards, G. T., & Stoughton, C. 1998, ApJS, 119, 121
Metcalfe, T. S. 2003, ApJ, 587, L43
Metcalfe, T. S., Salaris, M., & Winget, D. E. 2002, ApJ, 573, 803
Montgomery, M. H., Klumpe, E. W., Winget, D. E., & Wood, M. A. 1999, ApJ, 525, 482
Montgomery, M. H., & Winget, D. E. 1999, ApJ, 526, 976
Mukadam, A., et al. 2003a, in Proc. NATO Advanced Research Workshop on White Dwarfs, ed. D. De Martino (Dordrecht: Kluwer), 227
Mukadam, A. S., Winget, D. E., & Kepler, S. O. 2001, in ASP Conf. Ser. 226, 12th European Conf. on White Dwarf Stars, ed. H. L. Shipman et al. (San Francisco: ASP), 337
Mukadam, A. S., et al. 2003b, ApJ, 594, 961
Mukadam, A. S., et al. 2004, ApJ, submitted
Nather, R. E., & Mukadam, A. S. 2004, ApJ, 605, 846
Nitta, A., Kanaan, A., Kepler, S. O., Koester, D., Montgomery, M. H., & Winget, D. E. 2000, Baltic Astron., 9, 97
Nitta, A., Kepler, S. O., Winget, D. E., Koester, D., Krzesinski, J., Pajdosz, G., Jiang, X., & Zola, S. 1998, Baltic Astron., 7, 203
O'Donoghue, D., Kanaan, A., Kleinman, S. J., Krzesinski, J., & Pritchet, C. 2000, Baltic Astron., 9, 375
O'Donoghue, D., & Warner, B. 1987, MNRAS, 228, 949
Petersen, J. O., & Hog, E. 1998, A&A, 331, 989
Pier, J. R., Munn, J. A., Hindsley, R. B., Hennessy, G. S., Kent, S. M., Lupton, R. H., & Ivezić, Ž. 2003, AJ, 125, 1559
Robinson, E. L. 1979, in IAU Colloq. 53, White Dwarfs and Variable Degenerate Stars, ed. H. M. Van Horn & V. Weidemann (Rochester: Univ. Rochester Press), 343
Robinson, E. L., et al. 1995, ApJ, 438, 908
Salaris, M., Cassisi, S., García-Berro, E., Isern, J., & Torres, S. 2001, A&A, 371, 921
Scargle, J. D. 1982, ApJ, 263, 835
Smith, J. A., et al. 2002, AJ, 123, 2121
Standish, E. M. 1998, A&A, 336, 381
Stoughton, C., et al. 2002, AJ, 123, 485
Van Horn, H. M. 1968, ApJ, 151, 227
Vassiliadis, E., & Wood, P. R. 1993, ApJ, 413, 641
Warner, B., & Woudt, P. A. 2003, preprint (astro-ph/0310072)
Weidemann, V. 1990, ARA&A, 28, 103
Winget, D. E. 1998, J. Phys. Condensed Matter, 10, 11247
Winget, D. E., Hansen, C. J., Liebert, J., van Horn, H. M., Fontaine, G., Nather, R. E., Kepler, S. O., & Lamb, D. Q. 1987, ApJ, 315, L77
Winget, D. E., Hansen, C. J., & Van Horn, H. M. 1983, Nature, 303, 781
Winget, D. E., Kepler, S. O., Kanaan, A., Montgomery, M. H., & Giovannini, O. 1997, ApJ, 487, L191
Winget, D. E., et al. 2003, in ASP Conf. Ser. 294, Scientific Frontiers in Research on Extrasolar Planets, ed. D. Deming & S. Seager (San Francisco: ASP), 59
Wood, M. A. 1990, Ph.D. thesis, Univ. Texas at Austin
———. 1992, ApJ, 386, 539
Wu, Y., & Goldreich, P. 1999, ApJ, 519, 783
———. 2001, ApJ, 546, 469
York, D. G., et al. 2000, AJ, 120, 1579